THE IMPINGEMENT OF AXISYMMETRIC JETS ON PERPENDICULAR AND INCLINED PLANE WALLS

By

R. KANNAN

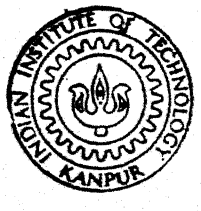

DEPARTMENT OF AEROSPACE ENGINEERING

INDIAN INSTITUTE OF TECHNOLOGY KANPUR

APRIL, 1993

THE IMPINGEMENT OF AXISYMMETRIC JETS ON PERPENDICULAR AND INCLINED PLANE WALLS

A Thesis submitted

in partial fulfilment of the Requirements

for the Degree of

MASTER OF TECHNOLOGY

by

R. KANNAN

to the

DEPARTMENT OF AEROSPACE ENGINEERING

INDIAN INSTITUTE OF TECHNOLOGY KANPUR

April, 1993

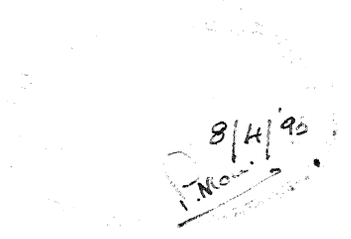

CERTIFICATE

It is certified that the work contained in the thesis entitled "*THE IMPINGEMENT OF AXISYMMETRIC JETS ON PERPENDICULAR AND INCLINED PLANE WALLS*", by R. Kannan, has been carried out under my supervision and that this work has not been submitted elsewhere for a degree.

(Dr. E. Rathakrishnan)
Dept. of Aerospace Engineering
I.I.T. Kanpur

April, 1993.

ABSTRACT

An experimental investigation of the jet issuing from a circular nozzle onto a plane surface, has been carried out for nozzle exit Mach numbers from 0.2 to 1.0 and underexpanded flow. Measurements of mean characteristics of the jet flow field were made when the jets impinge normally and obliquely on the smooth circular plate. The impingement flow field of the underexpanded jet is visualized using Schlieren - photography.

The results show that the presence of wall in the near field has significant effect on free jet characteristics. The wall surface pressure distribution identify two distinct zones: an 'influence zone' of high positive pressure and a 'zone of pressure fluctuations' of positive and negative pressures. The measurements of impinging jet characteristics indicate the presence of 'iso-Mach-lines' in the near and far fields. The wall surface pressure distribution of the impinging jet flow field is correlated with the mean characteristics of the free jet through intensity of impingement. In the oblique impingement, the maximum pressure on the wall when the wall is inclined can be larger than when the wall is perpendicular. From the Schlieren pictures, the wave structures of the free jet and impinging jet for underexpanded flow are quantified as far as possible.

DEDICATED

TO

MY FATHER

ACKNOWLEDGEMENT

I wish to acnowledge with sincere gratitude the invaluable guidance rendered by Dr. E. Rathakrishnan during the course of this thesis work. I would like to thank my colleague T. Ignatius without whose helpful dicussions and efforts, this work would not have been a success.

I gratefully acknowledge the interest and helpful comments of my friends Manoj and Vinayak during my thesis work. My special thanks to Justin Thomas and Solaiappan for preparing this report.

I would also like to thank Mr. Chauhan and Mr. Bhatu of the High Speed Laboratory, and Mr. Bhattacharya of the work shop for all their help throughout the experimental work.

Finally, I owe a debt of gratitude to all my family members for their encouragement and support in my studies.

R. Kannan

TABLE OF CONTENTS

	Page no.
List of figures	vii
Nomenclature	ix
1. Introduction	1
1.1 Literature Review	2
1.2 Applications	5
1.3 Aim of the present investigation	5
2. Experimental Programme	7
2.1 Experimental Apparatus	7
2.2 Experimental Procedure	8
3. Results and Discussion	10
3.1 Free jet Studies	10
3.2 Normal Impingement Studies	13
3.3 Oblique Impingement Studies	19
3.4 Discussion on Schlieren pictures	20
4. Concluding Remarks	22
References	24
Figures	26

LIST OF FIGURES

Figure 1. General features of jet flow. a) subsonic free jet
b) underexpanded free jet c) impinging jet

Figure 2. a) Schematic of the internal flow facility
b) Experimental arrangement for Schlieren system

Figure 3. Mean velocity profiles of free jet for M_e=0.8

Figure 4. Axial velocity decay of free jet

Figure 5. Variation of spread width of free jet along the axis

Figure 6. Entrainment of free jet

Figure 7. Axial velocity decay of impinging jet for M_e=0.4

Figure 8. Axial decay of pitot pressure of impinging jet for underexpanded flow

Figure 9. Measured spread of impinging jet along the axis for M_e=1.0

Figure 10. Entrainment of impinging jet for M_e=0.4

Figure 11. Entrainment of impinging jet for M_e=0.6

Figure 12. Entrainment of impinging jet for M_e=0.8

Figure 13. Mach number variation of impinging jet for M_e=0.4 and D_w=7.5d

Figure 14. Mach number variation of impinging jet for M_e=0.4 and D_w=20d

Figure 15. Wall surface pressure distribution on the plane of symmetry for M_e=0.4

Figure 16. Wall surface pressure distribution on the plane of symmetry for underexpanded flow

Figure 17. Variation of influence zone with wall distance
a) subsonic jets b) sonic and underexpanded jets

Figure 18. Wall surface pressure distribution for M_e=0.2

Figure 19. Wall surface pressure distribution for M_e=0.4

Figure 20. Wall surface pressure distribution for M_e=0.6

Figure 21. Wall surface pressure distribution for M_e=0.8

Figure 22. Wall surface pressure distribution for M_e=1.0

Figure 23. Wall surface pressure distribution for underexpanded flow

Figure 24. Comparison of wall surface pressure distribution with theory

Figure 25. Comparison of free jet and wall surface pressures for M_e=0.4.

Figure 26. The intensity of impingement correlated with free jet data for M_e=1.0
a) radial variation b) axial variation

Figure 27. Wall surface pressure distribution for oblique impingement at various D_w
a) M_e=0.8 and α=85° b) M_e=0.8 and α=80°
c) M_e=0.8 and α=75° d) underexpanded flow and α=85°
e) underexpanded flow and α=80° f) underexpanded flow and α=75°

Figure 28. Wall surface pressures for oblique impingement at D_w=5d and M_e=0.4

Figure 29. Wall surface pressures for oblique impingement at D_w=5d and M_e=0.6

Figure 30. Wall surface pressures for oblique impingement at D_w=5d and M_e=0.8

Figure 31. Wall surface pressures for oblique impingement at D_w=5d and M_e=1.0

Figure 32. Wall surface pressures for oblique impingement at D_w=5d and underexpanded flow

Figure 33. Axial distribution of pitot pressure of free jet for underexpanded flow

Figure 34. Schlieren picture of free jet

Figure 35. Schlieren pictures of normally impinging jet
a) D_w=1d b) D_w=2d c) D_w=2.5d d) D_w=5d

Figure 36. Schlieren pictures of obliquely impinging jet
a) α=85° and D_w=2d b) α=85° and D_w=2.5d

Figure 37. Schlieren pictures of obliquely impinging jet
a) α=85° and D_w=5d b) α=80° and D_w=5d c) α=75° and D_w=5d

NOMENCLATURE

b - spread width at which U=$U_j/2$

C_p- intensity of impingement upon wall

d - exit diameter of nozzle

D_w- distance from nozzle exit to wall

I_d- influence diameter

M_e- jet exit Mach number

M_I- iso-Mach number

P - static pressure in jet flow field

P_a- ambient atmospheric pressure

P_c- pressure at wall centre

P_{max}- peak wall pressure on the inclined wall

P_o- measured total pressure in jet flow field

P_p- measured pitot's pressure in jet flow field

P_w- wall surface pressure

Q - flow rate at any section normal to the jet axis

Q_o- flow rate at nozzle exit

r - radial distance from jet axis

r_M- iso-Mach-line location along r

U - jet velocity at any radial distance r

U_j- free jet centre-line velocity

U_e- nozzle exit velocity

x - distance along jet axis

α- angle of wall inclination with respect to jet axis

CHAPTER 1

INTRODUCTION

The problem of jet impingement arises when a jet of fluid strikes over a surface. In the case of single jet impingement on a flat surface either normally or obliquely, the flow field consists of three regions: free jet region, impingement region and wall jet region.

The general features of subsonic free jet flow, consisting of the potential core, the mixing region, the transition region and the fully developed region, are as shown in Fig 1a. The subsonic jet is characterized by the potential core surrounded by the mixing region where the mixing between the jet and surrounding fluid takes place. A few nozzle diameters downstream, the mixing region spreads inward enough to reach the jet centre-line and core no longer exists. Beyond this point, the mean velocity profiles approach the self-similar shape of the fully developed flow.

For subsonic free jet flow, the pressure ratio $\frac{P_o}{P_a}$ is below the critical value of 1.89. When the pressure ratio is equal to 1.89, the flow becomes correctly expanded with sonic exit. If this pressure ratio is above the critical value, the nozzle exit static pressure is no longer equal to ambient pressure. The jet flow for which the exit pressure is above the ambient pressure, is termed as "underexpanded flow". If the pressure ratio is within the interval 2 to 3.8, then the jet flow is called "moderately underexpanded flow". In this type of flow with sonic exit, the familiar pattern of 'shock diamonds' or 'cells' composed of intersecting oblique shocks is established in the near field as shown in Fig 1b.

The different zones of normally impinging jet flow field, as shown Fig 1c, are:

1. 'Free jet zone' which starts from the exit of the nozzle to some distance above the solid surface;

2. 'Impingement zone', the zone from the axial location at which the velocity decay begins to deviate from that of free jet, up to the solid surface. The velocity is reduced to zero at the stagnation point on the solid surface. The stagnation pressure is significantly higher than the ambient pressure which enables a favourable pressure gradient along the direction tangent to the wall resulting the flow to proceed as a wall jet radially outwards;

3. 'Wall jet zone' which consists of essentially radial flow along the wall surface and the magnitude of the pressure is close to the ambient pressure value.

However, for oblique impingement the entire impingement and wall jet flow fields are asymmetrical and the location of the stagnation point need not be at the centre of wall.

1.1 LITERATURE REVIEW

This review , in an attempt to collect related systematic and chronological studies, includes experimental and theoretical works which are relevant to the present investigation.

Donaldson and Snedeker [1] studied both normal and oblique jet impingement on various surface shapes for subsonic, moderately underexpanded and highly underexpanded jets issuing from a circular, convergent nozzle. They correlated the measured distribution of surface pressure with local mean properties of the free jet. It was found that for normal impingement, the radial velocity gradient computed at the stagnation point using surface pressure distribution correlates with free jet centre-line velocity and half-radius at the same axial location.

Gummer and Hunt [2] investigated the impingement of a uniform, axisymmetric, supersonic jet on a flat plate both experimentally and theoretically for four different Mach numbers in the range 1.6 to 2.77. The centre-line shock height was determined theoretically using Polynomial Approximation Integral Relation method and was found to be in good agreement with experimental results. A qualitative description of the complex region involving the sonic line and the beginning of the wall jet was given. Bradbury [3] studied the impact of an

axisymmetric jet onto a normal ground. He presented an argument for correlating the data obtained in the impact region from different nozzle configurations and for different nozzle heights above the ground. In particular the argument was applied to the peak dynamic head in the flow over the ground board. From the experiments done, it was concluded that there is no significant effect of Reynolds number between his tests and full scale.

Carling and Hunt [4] presented detailed measurements of the surface pressures and shadowgraph pictures in the study of supersonic jet impingement on a flat surface. The mechanism of supersonic near wall jet was found to consist an alternating series of expansion and recompression regions. Pollard and Bradbury [5] presented a brief report about the experimental work on rectangular supersonic jets impinging upon a normal ground surface. The pressure distribution on the ground surface under the impinging jet was correlated for various nozzle heights above the ground on the basis of free jet characteristics.

The work carried out by Gutmark et al. [6] was on the experimental study of the turbulent structure on the centre-line of a two dimensional impinging jet. They found that the flow properties on the centre-plane of the impinging jet are essentially the same as that of a free jet except in a short region in front of the solid surface. Their spectral measurement detected a frequency range in which turbulent energy is neither augmented nor attenuated.

Lamont and Hunt [7] have reported an extensive experimental study of the flows due to underexpanded, axisymmetric jets impinging on flat plates. In oblique impingement, plate inclinations from 90° to 30° were investigated by means of comprehensive surface pressure measurements and shadowgraph pictures. They found that the interactions between the shock waves in the free jet and those created by the plate have very strong influences on the surface pressures measured on the plate. It was concluded that the maximum pressure on the plate when it was inclined can be much larger than when the plate is perpendicular. The overall integrated pressure loads on the plate for different plate inclinations were found to be predicted reasonably well by a simple momentum balance.

Chich-ming Ho et al. [8] presented surface pressure fluctuations when a high speed sub-

sonic jet impinges on a flat plate. These pressure fluctuations which have a broad spectrum due to turbulent nature of the high Reynolds number jet, dramatically change their pattern into almost periodic waves when the plate is close to the nozzle. Katok et al. [9] studied mass transfer rate and velocity gradient when an axisymmetric jet impinges on a flat plate. The local measurements of surface pressure were done using piezo-electric pressure transducers. They found that the surface pressure turbulence is generated by the impinging jet from the velocity turbulence of the oncoming jet.

The numerical investigation carried out by Hwang et al. [10] was about the flow and heat transfer in an incompressible plane turbulent jet impinging obliquely on a flat surface. They concluded that the shift in stagnation point from the intersecting point of the jet centre-line with surface decreases as Reynolds number increases. Looney et al. [11] investigated mean flow and turbulent characteristics of impinging jet flows numerically. It was found that the developing wall jet resulting from the plane impinging jet, is identical with standard wall jet configuration.

Iwamoto [12] studied the flow pattern of underexpanded impinging jet both numerically and experimentally for pressure ratios ($\frac{P_o}{P_a}$) 3 and 6. Measurements of surface pressure on the plate revealed that the maximum pressure does not occur at the centre of the plate and that a region of reversed flow exists near the centre.

Though fairly large number of investigations on the problem of jet impingement is available, the mechanism close to the impinging surface has not yet been well established. There is very little information available about the near field jet impingement. In order to understand the phenomenon of jet impingement, the present study is concerned with impingement both in the near and far fields. Also, it is necessary to study important parameters like influence zone on the wall surface, intensity of impingement, effect of wall on jet entrainment and so on to obtain the complete information about the behaviour of impinging jets.

1.2 APPLICATIONS

Impinging jets are of great and diverse engineering importance and the task of preparing a complete list of examples, together with the field concerned, is of itself a major undertaking. While some of the best known and most challenging applications lie in the field of aerodynamics, these roles are far outweighed in number and economic importance by the use of impinging jets in other fields like heating, cooling, cutting of metals and so on. Some of the important applications are listed below:

1. jet engine exhaust impingement of *V/STOL* aircraft;
2. effective film-cooling of gasturbine combustion chamber wall and the leading stages of the turbine;
3. boundary layer control in aerofoil sections by blowing air through the leading edge slots;
4. terrestrial rocket launch and design of launchers;
5. jet-spray painting at low velocities;
6. removal of thin surface layers;
7. toughening of glass;
8. drying of textiles and paper.

It is clear from the examples cited above that a thorough knowledge of fluid mechanics of the impinging jet can materially improve the design of such devices.

1.3 AIM OF THE PRESENT INVESTIGATION

An experimental study of jet issuing from a convergent, circular nozzle, impinging onto a plane surface for subsonic, sonic and moderately underexpanded flow with pressure ratio $\frac{P_o}{P_a} = 2.5$, has been carried out. In the present study, most attention is given to normally

impinging jets and it is also proposed to study some aspects of obliquely impinging jets. The present investigation includes the following:

1. The mean characteristics of free jet;
2. The influence of wall on the free jet characteristics: axial velocity decay, spread width, virtual origin and entrainment;
3. The mean Mach number profiles of impinging jet flow field;
4. The various zones of wall surface pressure distribution in the normal impingement study;
5. The influence of plate inclination on wall surface pressure distribution in the oblique impingement study;
6. The wave structure in the free jet and the influence of wall on the behaviour of shock cells using Schlieren pictures.

CHAPTER 2

EXPERIMENTAL PROGRAMME

2.1 EXPERIMENTAL APPARATUS

The experiments on jet impingement were carried out with jets issuing from an axisymmetric, convergent, circular nozzle of 10 mm exit diameter. The nozzle used was of faired entry with inlet diameter 30 mm and thickness 25 mm. The experiments were done using internal flow facility, at the High Speed Aerodynamics Laboratory of IIT Kanpur. The experimental apparatus is shown schematically in figure 2a. The jet from the nozzle at different Mach numbers, achieved by controlling the stagnation pressure in the settling chamber, was made to impinge normally on a smooth circular plate. The temperature in the settling chamber was measured using a mercury thermometer. The plate was provided with pressure tappings spaced 5 mm apart, arranged along a diameter for the measurement of wall surface pressure distribution. There were 56 pressure tappings of 0.7 mm diameter on the perspex plate which is of 12 mm thickness and 300 mm diameter. The plate was mounted on a rigid one-dimensional traverse used to vary the nozzle to plate distance.

The pressure measurements in the jet field was made using a total pressure probe of 0.8 mm inner diameter mounted on a traversing mechanism having six degrees of freedom with a least count of 0.1 mm in linear and 0.5 degree in angular measurements. Long column 'U' tube mercury manometer for total pressure measurements and multi-tube mercury manometer for wall surface pressure measurements were used.

Schlieren technique was used to visualize the wave pattern in the jet flow field. Typical Schlieren system using concave mirrors, is shown in figure 2b. In this setup, a source of light at the focus of the concave mirror M_1, sends parallel rays of light through the near field

of the nozzle exit. A second mirror M_2 focuses the on-coming rays to a knife edge which controls the intensity of light on the screen. When there is no flow, all the rays emanating from the source condense at the knife edge, thereby producing a uniform illumination on the screen. But, when there is underexpanded flow, there are shock waves and expansion waves in the near filed, producing regions of higher and lower density. The rays passing through the jet flow field undergo different orders of refraction and regions of dark and bright patches appear on the screen representing the shock and expansion waves.

2.2 EXPERIMENTAL PROCEDURE

Compressed dry air at high pressure stored in reservoirs with 3000 ft^3 capacity, was made to expand through a gate valve and Pressure Regulating Valve (PRV) before attaining an equilibrium in the settling chamber. The pressure in the settling chamber was measured by a Bourdon type pressure gauge and a long column 'U' tube mercury manometer.

Any required pressure in the settling chamber was achieved by controlling the PRV and was allowed to expand through the nozzle, which discharged into the ambient atmosphere. The different jet Mach numbers of the present study were attained by controlling the pressure in the settling chamber at different levels. The experiment was done in the pressure range $(\frac{P_o}{P_a})$ 1.03 to 2.5.

2.2.1 NORMAL IMPINGEMENT

The experiments were carried out for jet exit Mach numbers of 0.2, 0.4, 0.6, 0.8 and 1.0, and for underexpanded flow with pressure ratio, $\frac{P_o}{P_a} = 2.5$. The corresponding range of Reynolds number based on nozzle exit diameter is from 48,000 to 240,000. The circular plate was mounted on the one-dimensional traverse. In the case of normal impingement, the wall was kept normal to the jet axis and the centre of the wall was aligned to the jet axis. The nozzle to plate distance was varied from 2.5d to 30d and measurements were made. The pressure tappings on the plate were connected to the multi-tube mercury manometer and wall surface pressure measurements were made. The total pressure measurements in the

impinging jet flow were made by traversing the total pressure probe radially at every station along the jet axis. Since each free jet at a particular Mach number has its own characteristics and the nature varies for different ambient conditions, the experiment was carried out with impinging jet study followed by the free jet measurements for the corresponding nozzle exit Mach number. The free jet was calibrated up to 30d from the nozzle exit by traversing the total probe radially in steps of 1d along the jet axis. In impinging jet and free jet studies, the total probe was moved radially in the horizontal direction at every 1 mm, keeping the probe in the direction of jet axis.

2.2.2 OBLIQUE IMPINGEMENT

In oblique impingement, three different angles of 75°, 80° and 85° with respect to the jet axis were considered. Due to the interaction of the wall with the end plate of the wind tunnel, the inclination was limited to 75° and the wall was located beyond 5d. Particular inclination of the wall was achieved using the rotation of the vertical rod supporting the plate. The wall distance was varied from 5d to 30d for different nozzle exit Mach numbers of 0.4, 0.6, 0.8 and 1.0, and for underexpanded flow with pressure ratio ($\frac{P_o}{P_a}$) 2.5. Only wall surface pressure measurements were made when the wall was located at a particular axial distance.

Whenever the pressure reading on the manometer was found oscillating, mean value was taken. The measured accuracy of the manometer was of 0.5 mm mercury. The maximum variation of temperature in the settling chamber during the runs were of the order of 1°C , therefore, the temperature has been assumed constant.

2.2.3 SCHLIEREN PICTURES

Schlieren photographs of the jet flow in the near field with and without wall were taken for moderately underexpanded flow with $\frac{P_o}{P_a} = 2.5$. In the normal impingement studies, the range of wall locations extends to 5d from the nozzle exit. The jet flow fields with the wall inclined at three different angles of 85°, 80° and 75° at 5d were also captured. At one particular inclination of 85°, the wall distance was varied from 2d to 5d and the flow patterns between the nozzle exit and the wall were visualized.

CHAPTER 3

RESULTS AND DISCUSSION

The measured data consist of mean total pressure at different nodal points of the jet field. The Mach number M at those points is calculated for subsonic and sonic flow using the isentropic relation given below:

$$\frac{P_o}{P_a} = \left(1 + \frac{\gamma - 1}{2} M^2\right)^{\frac{\gamma}{\gamma - 1}} \tag{1}$$

where P_o is the local total pressure of the fluid after it was slowed down isentropically to zero velocity

P is the local static pressure of the fluid

γ is the specific heat ratio of the fluid.

For jet flow with pressure ratio $(\frac{P_o}{P_a})$ below the critical value of 1.89, the static pressure throughout the flow can be assumed to be equal to ambient atmospheric pressure.

The axisymmetry of both free jet flow and impinging jet flow has been verified by carrying out the measurement on both sides of the axis. A large amount of data has been obtained in order to analyse all the important parameters which are considered to be most useful to the engineer. The data processing was done on Hewlett Packard 9000 computer. All the results are presented in the form of dimensionless parameters.

3.1 FREE JET STUDIES

3.1.1 Mean Mach number profiles

In the present study, in order to correlate the impinging jet flow field, it is necessary to investigate the characteristics of the free jet. The free jet flow field is calibrated using total probe up to 30d from the nozzle exit. The mean velocity profiles in the radial direction both

in the near and far fields are shown in figure 3. Tollmien's theoretical curve is also included for comparison. The velocity is found to be uniform near the centre-line in the core region and the profiles are self-similar after x = 9d where flow is said to be fully developed.

3.1.2 Axial velocity decay

In the general structure of the free jet, it is well known that the potential core where the axial velocity is retained, extends up to few nozzle diameters from the exit. Beyond the potential core, the velocity decays at a rate required to conserve axial momentum. The measured axial velocity decay of the free jet is shown in figure 4. Tollmien's velocity decay scale [13] for free jets based on Prandtl's mixing length hypothesis, is given as

$$\frac{U_j}{U_e} = 7.32\frac{1}{x/d} \tag{2}$$

where the constant relates the shear stress and mixing length in the hypothesis. The above axial velocity decay scale is plotted along with the measured experimental data (figure 4). The experimental results show the same trend as the Tollmien's decay except for higher Mach numbers. This could be attributed to the incompressibility assumption imposed in the Tollmien's formula. It is also inferred that downstream of x = 15d, the decay for all Mach numbers follows the Tollmien's theoretical solution quite closely.

3.1.3 Half-spread width

The Half-spread width is defined as the radial distance from the jet axis where the velocity is equal to half of the axial velocity. The variation of spread of the free jet along the axis is shown in figure 5. It can be seen that the spread decreases as the Mach number increases from 0.2 to 1.0. Tollmien's variation of spread is also plotted for comparison. The value of spread rate $\frac{db}{dx}$ for incompressible Mach number is in good agreement with Tollmien's value of 0.082. However, for compressible flow the rate of spread of the free jet decreases from 0.077 for M_e= 0.4 to 0.066 for M_e= 1.0.

3.1.4 Virtual origin

The virtual origin, defined as the imaginary location from where the jet seems to emanate,

was calculated from the variation of half-spread width and it is estimated to be at x/d = -2.56. The length of the core from the virtual origin is found to be 7.56d. Even though this is less than theoretical value of 8.0d, it agrees well with Donaldson's [1] experimental value of 7.5d.

3.1.5 Entrainment

One of the important characteristics of free jet flow field is the entrainment. The flow rate Q is known to increase with distance x from the nozzle exit. The fluid from the surroundings is drawn radially inwards towards the jet across its conical boundary surface; this process is known as 'entrainment'. The flow rate Q at any section is given by

$$Q = \int_0^{r_0} 2\pi r U dr \tag{3}$$

where r_o is the radial distance up to the jet boundary.

If Q_o is the flow rate at the nozzle exit, it is known from experiments that $\frac{Q}{Q_o}$ is proportional to x, when the distance x is much larger than the diameter of the nozzle.

$$\frac{Q}{Q_o} = kx \tag{4}$$

where k is known as the entrainment constant.

The entrainment parameter $\frac{Q}{Q_o}$ is plotted as a function of x in figure 6. The flow rate Q at any section was calculated using numerical integration. The entrainment is found to increase almost linearly with distance x along the direction of jet axis. It is clearly inferred from the figure that the increase in Mach number from 0.4 to 0.6 results in enhancement of entrainment. The computed value of entrainment constant k is 0.35 which is close to the experimental value of 0.32 reported by Ricou and Spalding [14]. After 15d, the entrainment does not show any orderly behaviour and the reason for this behaviour may be explained as follows : It is difficult to measure the total pressure accurately at larger radial distance and the presence of r as a multiplier of U in equation 3 augments the influence of inaccuracies in this region.

3.2 NORMAL IMPINGEMENT STUDIES

In the present work, attention is focused mainly on the study of normally impinging jets. The flow field of normally impinging jet includes the free jet upstream of the wall, the influence zone near the wall centre and the wall jet zone, as shown in figure 1c. The influence of wall on free jet characteristics, the mean characteristics of impinging jets flow field and the distribution of wall surface pressures are discussed in this section.

3.2.1 INFLUENCE OF WALL ON FREE JET CHARACTERISTICS

The measurements of the mean properties of the impinging jet flow field for various wall distances are presented. In order to analyse the influence of wall on free jet characteristics, the variations of all the parameters in the impinging jet flow field is plotted along with that of free jet.

The axial velocity decay for various wall distances D_w is plotted in figure 7, along with that of the free jet for comparison. It is seen that the presence of wall has only a marginal influence on the centre-line velocity decay even for the wall locations close to the nozzle exit. Nosseir [15] also reported similar results and he found that the free jet centre-line velocity was influenced only downstream of $0.84D_w$ due to the presence of wall.

The axial distribution of pitot pressure in the impinging jet flow field for underexpanded jet is presented in figure 8. It should be noted that in the underexpanded jet, the flow becomes complex in the near field and the pattern of 'shock diamonds' composed of intersecting oblique shocks is established. Hence the total pressure readings cannot be converted into velocity, the reading not being the actual pressure values. The decay of pitot pressure shown in figure 8 is clearly indicative of the kind of axial variations to be expected in the near field. The results are in good agreement with that of Donaldson et al [1]. The effects of underexpansion can be clearly seen. However, the measured data points which represent supersonic flow in the near field may not be sufficient to show detailed core structure because of the local pressure variations within the length of each shock cell. The effect on decay of pitot pressure due to the presence of wall is felt only up to a very short distance from the

wall, as seen from figure 8.

The variation of spread with axial distance in the impinging jet flow field is non-linear as shown in figure 9. The spread is higher than that of the free jet in the region close to the wall. Beyond D_w= 15d, even though the effect of wall is felt for a larger upstream distance, the magnitude of this effect is only marginal. The trend appears to be the same for all Mach numbers of the present study.

The virtual origin was calculated based on half-spread width for the impinging jet. The travel of virtual origin with with wall distance is shown in table 1.

Table 1. Movement of the virtual origin with D_w

D_w	Virtual origin
5d	-28.3
10d	-25.4
12.5d	-16.1
15d	-11.0
20d	- 6.2
25d	- 3.1
free jet	- 2.56

The location of virtual origin calculated based on above criteria appears to be very sensitive to the wall distance. It is generally found that it is located upstream of the nozzle exit for all wall distances of the present study. For D_w beyond 20d, the deviation of virtual origin from that of free jet becomes narrow showing a tendency to merge with that. The movement of virtual origin with D_w seems to be independent of Mach numbers.

In order to obtain complete information about the effect of the presence of wall on free jet characteristics, it is necessary to investigate its influence on free jet entrainment. Analysis of lift losses due to entrainment is of critical importance in the design and development of *V/STOL* aircraft. The entrainment study was made for Mach numbers 0.4, 0.6 and 0.8. The variation of flow rate Q for various D_w is plotted in figures 10 to 12. It is seen that the entrainment decreases for all wall locations and the same trend is observed for all Mach numbers.For M_e=0.4, the maximum decrease was 25% and it occurred at x/d =12 for

D_w=15d. A maximum decrease of 41% was found for M_e=0.6 at x/d =12.5 for D_w=15d. For M_e=0.8, the reduction in entrainment registered a maximum of 40% at x/d =11 for D_w=15d. For above three Mach numbers, the average value of entrainment constant was found to be 0.21, 0.15 and 0.21 respectively.

3.2.2 MACH NUMBER CONTOURS

The mean Mach number profile is one of the important characteristics of impinging jet flow field. In this section, the measured Mach number contours of impinging jet for different combination of parameters are presented. The measured Mach number variation along the jet radial direction at various axial stations , for a given D_w is presented in figures 13 and 14. From figure 13, it is seen that the velocity decay along r in the impinging jet flow field exhibits a single crossover point at r = r_M. This indicates the existence of a constant Mach number line at r_M along x, defined as 'iso-Mach-line'. The crossover point r_M and iso-Mach-line Mach number M_I are found to be sensitive to wall distance D_w. As D_w increases, the crossover point diffuses slightly and for larger D_w, two crossover points, one in the free jet zone and the other in the impingement zone, are observed as shown in figure 14.

The behaviour of the iso-Mach-lines for various D_w and M_e can be seen from table 2. The crossover points reveal that it is a point at which the radial isobars cross over.

Table 2. Behaviour of crossover point and iso-Mach number.

a) Impinging jet zone

D_w	M_e=0.4		M_e=0.6		M_e=0.8		M_e=1.0	
	r_M/d	M_I	r_M/d	M_I	r_M/d	M_I	r_M/d	M_I
7.5d	0.55	0.22	0.52	0.38	0.60	0.40	0.75	0.40
10d	0.50	0.20	0.50	0.25	0.60	0.36	0.45	0.66
12.5d	0.72	0.18	0.76	0.24	0.70	0.32	0.70	0.43
15d	—	—	0.80	0.20	1.0	0.26	0.60	0.46
20d	1.25	0.09	1.10	0.16	1.10	0.25	1.00	0.30
25d	1.05	0.11	1.00	0.15	1.10	0.20	1.10	0.27
30d	—	—	1.50	0.11	1.50	0.16	1.45	0.24

b) Free jet zone

D_w	M_e=0.4		M_e=0.6		M_e=0.8		M_e=1.0	
	r_M/d	M_I	r_M/d	M_I	r_M/d	M_I	r_M/d	M_I
15d	0.60	0.20	0.50	0.33	0.50	0.44	0.50	0.65
20d	0.45	0.29	0.70	0.23	0.70	0.34	0.60	0.46
25d	0.60	0.21	0.65	0.22	0.60	0.38	0.60	0.38
30d	—	—	0.70	0.11	0.65	0.34	0.70	0.45

3.2.3 WALL SURFACE PRESSURE DISTRIBUTION

The study of wall surface pressure distribution covering the entire impingement region and wall jet region, includes different zones in the wall surface pressure distribution, the comparison of wall surface pressures with free jet mean pressure distribution and the intensity of impingement C_p. An attempt was made to correlate the wall surface pressure distribution with local mean characteristics of the free jet for different nozzle conditions and wall distances.

The variation of wall surface pressure along the radial direction in the plane of symmetry is presented in figures 15 and 16. It is observed that the region around the wall centre is dominated by maximum positive pressure. In the case of underexpanded jet, the stagnation pressure decays along the axial direction at a faster rate compared to the other cases, as seen from figure 16. This could be due to the loss of pressure through the wave dominated structure. The zone of maximum positive pressure extending up to the location where $\frac{P_w}{P_a} = 1.0$ is defined as the 'zone of influence' of impingement. The diametrical extent of this zone is termed as the 'influence diameter' I_d.

The variation of the influence diameter along the jet axis for subsonic, sonic and underexpanded flow is given in figures 17. From these figures it is seen that there is a sharp increase in I_d for smaller D_w and for Mach numbers from 0.4 to 1.0. However, for Mach 0.2 I_d is independent of D_w. For all Mach numbers influence diameter is almost constant for wall distance D_w beyond about 7.5d as expected, since the jet becomes self-similar. However,

the behaviour of I_d with D_w is different for underexpanded jet. The influence diameter is almost constant up to D_w = 15d, and then it increases drastically, reaching a maximum value of 12.5d at D_w = 30d as shown in figure 17b. This shows that the radial variation of wall surface pressure is more gradual, showing a monotonic increase in the far field, as seen from figure 16.

Beyond influence zone, there is a 'zone of pressure fluctuations' between positive and negative values, as shown in figures 18 to 23. These oscillations are critical in fatigue of the impingement surface. Carling and Hunt [4] also reported a similar trend of these fluctuations extending radially along the wall surface at supersonic jet Mach numbers in the range 1.64 to 2.77. The negative peak pressure increases in magnitude with increasing M_e. For a particular Mach number, the location of the negative peak pressure is almost same for various D_w, as seen from figures 18 to 23.

Rajarathnam [13] established analytical expressions for radial as well as axial decay of wall surface pressures. He found that the radial pressure distribution on the wall could be represented by the equation

$$\frac{P_w}{P_c} = exp[-114(r/D_w)^2] \tag{5}$$

where P_w is the excess wall pressure above that of the ambient.

The expression for axial decay of stagnation pressure above that of the ambient pressure was given as

$$P_c = \frac{50}{(D_w/d)^2}\frac{\rho U_e^2}{2} \tag{6}$$

Comparison of the radial and axial distribution of wall pressures calculated using the above equations was made with the measured experimental pressure distribution, in figure 24. The present results are in excellent agreement with that of Rajarathnam. However, the trend of axial distribution of pressures below 7.5d differs due to the fact that the stagnation pressure tends to infinity as D_w in equation 5 approaches zero.

Comparison of the free jet mean pressure distribution with wall surface pressure distribution for various D_w is given in figure 25. From this figure it is seen that the pressure distribution near the centre of the wall is lower in magnitude than that of the free jet. However, beyond the crossover point, this behavior is reversed at a particular plane. The results reveal that the radial momentum of the free jet is enhanced by the presence of wall for D_w up to 15d. It is also observed that in the far field, the mean pressure of free jet is slightly less than the wall surface pressure in the central portion. Similar trend was reported by Bradbury [3] for exit velocity 120 m/sec and his results indicate that there was 12% increase in wall stagnation pressure over free jet mean pressure at the centre for particular wall location in the far field. In the present study, the maximum increase of wall stagnation pressure is about 16% registered at M_e= 1.0 for D_w= 20d.

The wall surface pressure distribution has been correlated with local dynamic pressure of the free jet through a parameter referred to as 'intensity of impingement' C_p. C_p was calculated using the following equation:

$$C_p = \frac{P_w - P_a}{P_j - P} \tag{7}$$

The variation of C_p for different wall distances is shown in figures 26. It is interesting to note that the intensity of impingement increases with increasing D_w, attains maximum and decreases with further increase of D_w, as seen from figure 26b. This behaviour of C_p is insensitive to Mach number. The above behaviour of C_p could be due to the following reason: in the near field the momentum of the jet has to change its direction within a short distance thereby resulting in a sharp turn of streamlines towards the outer zone. The entire field including the streamline of the jet axis was influenced by this behaviour, which results in a reduction of centre-line wall pressure compared to the free jet value. However, in the far field the change in direction of jet momentum is taking place over a large area and the centre-line pressure is not influenced by the presence of wall. Table 3 gives the variation of wall distance D_w for which the intensity of impingement is maximum. In the present study, the behaviour of $C_{p_{max}}$ location shows a trend for highly compressible subsonic and

The axial location of $C_{p_{max}}$ shows a tendency to shift towards the nozzle exit and this could be due to the fact that the inertia effects are predominant as the Mach number increases.

Table 3. Behaviour of intensity maximum.

Exit Mach number,M_e	D_w for which C_p is maximum
0.2	10d
0.4	25d
0.6	7.5d
0.8	25d
1.0	20d
underexpanded jet	15d

3.3 OBLIQUE IMPINGEMENT STUDIES

The study of obliquely impinging jets is principally concerned with the distribution of wall surface pressures along a diameter which is orthogonal to the axis of rotation. The investigation includes the wall surface pressure distribution for various wall distances at a particular inclination of the wall with respect to the jet axis and the effect of wall inclination on the distribution of wall surface pressures at various wall locations.

Figures 27 represent the general behaviour of the obliquely impinging jets as the wall distance D_w increases, for a particular angle of inclination α. The smooth radial distribution of wall surface pressures shows that the peak pressure occurs slightly away from the wall centre. As D_w increases, the shift from the centre increases for a particular angle of wall inclination. In the case of underexpanded jet, the maximum pressure decays at a faster rate along the axial direction compared to the other cases. Also, it is observed from the figure 27e that a wavy pattern is developed for underexpanded jet after 10d at $\alpha = 80°$. A similar pattern was reported by Lamont and Hunt [7] at a pressure ratio close to the present one.

The radial distribution of wall pressures for D_w= 5d at various inclinations of 85°, 80° and 75° for different Mach numbers are plotted in figures 28 to 32. The wall surface pressure distribution for normal impingement is also given for comparison. A general point of some

importance which arises from these results is that the maximum pressure on an inclined wall can be higher than that on a perpendicular wall. In the present range of inclination, the largest pressure was 7% above the normal impingement value, registered at M_e= 0.8. There is a pronounced effect on of wall inclination on maximum pressure for lower Mach numbers, as seen from the figures 28 and 29. There is an increasing trend of maximum pressure for M_e= 0.4 and 0.6 as α decreases whereas, the above trend is reversed in the case of higher Mach numbers. Table 4 gives an idea about the behaviour of peak pressure as a function of inclination angle α. From the results of wall surface pressure distribution in the far field, which are not presented here, it is found that the peak pressure first increases and then decreases as the angle of inclination α decreases from 85° to 75° for all Mach numbers.

Table 4. Behaviour of peak pressure with wall inclination

Exit Mach number,M_e	Inclination angle α (deg)	Peak pressure P_{max}/P_c	Radial location r_m/d
0.4	85	1.026	0.94
	80	1.025	1.40
	75	1.01	2.30
0.6	85	1.06	0.94
	80	0.97	1.37
	75	1.04	2.31
0.8	85	1.04	0.94
	80	1.07	1.37
	75	1.06	1.81
1.0	85	0.97	0.94
	80	1.05	1.37
	75	0.99	1.81
under-expanded flow	85	0.91	0.94
	80	1.01	1.31
	75	0.96	2.31

3.4 DISCUSSION ON SCHLIEREN PICTURES

The near flow fields of the free jet and the impinging jet were visualized using Schlieren-photography. The study of Schlieren pictures includes the wave structure of free jet in the near field and the effect of presence of wall on the behaviour of the shock cells.

Figure 34 shows the Schlieren picture of free jet and from this picture the overall wave

structure in the near field was determined as far as possible. It is seen from the figure that the Mach disk or normal shock crossing is not well formed since the degree of underexpansion of the jet is not high enough. The cellular structure of the free jet is apparently seen. Mach disks are identified at axial distances 1.1d, 2.6d and 3.7d. Distribution of pitot pressure along the jet axis is shown in figure 33 where the location of the Mach disks, as seen on the Schlieren picture, is also shown.

The Schlieren picture of the normally impinging jet when the wall is located at 1d from the nozzle exit is shown in figure 35a. A bow shock which is convex upwards can be seen in front of the wall at 0.8d from the nozzle exit and the flow pattern upstream of the bow shock is similar to that of the free jet. The convex upwards of this plate shock could be due to the stagnation zone at the wall centre. The flow immediately after this bow shock is subsonic. when the wall is moved to 2d, the shock moves together with the wall (figure 35b) . When its position coincides with that in the free jet, it remains at this position and downstream of it another shock appears. The shape of this shock wave located closer to the wall is almost normal. When the wall is moved further from the nozzle, there are two Mach disks in the free jet zone and a plate shock in front of the nozzle (figure 35c), which is not very clearly seen. At D_w= 5d, the presence of wall appears to be insensitive to the shock patterns as seen from figure 35d. The reduction of shock length due to the presence of wall for D_w below 5d may be due to the loss of relaxation freedom for the jet when the wall is present.

In the oblique impingement, the study includes the effect of wall inclination and the movement of wall at a particular angle on the shock structure. when the wall is inclined at $\alpha = 85^{\circ}$ with D_w= 2d, a Mach disk and a plate shock near the wall were seen (figure 36a). The lower edge of the plate shock is almost lost in the edge shear layer. As the wall is moved to 2.5d, the Schlieren picture (figure 36b) contains a dark and rather blurred region near the wall where the shock might be expected to lie. The effect of wall inclination on the shock structure at D_w= 5d is almost negligible as seen from figures 37.

CHAPTER 4

CONCLUDING REMARKS

An extensive study of the impingement of axisymmetric jets on perpendicular and inclined plane walls has been conducted. The following conclusions are drawn based on the results obtained.

1. The free jet characteristics: virtual origin and entrainment are influenced by the presence of wall significantly. However, the effect of wall on spread width and velocity decay after Dw=15d is only mariginal.

2. The impinging jet flow field characterize the existence of iso-Mach-lines and the crossover point diffuses into two as the wall distance increases.

3. In the distribution of wall surface pressures there are two distinct zones: 'influence zone' of maximum positve pressure and 'zone of pressure fluctuations' between positve and negative values. The trend of influence zone is almost similar for exit Mach numbers from 0.4 to 1.0. However, there is drastic increase of influence zone in the far field for underexpanded flow. The magnitude of pressure fluctuations is found to increase with increase of exit Mach number.

4. The intensity of impingement increases with wall distance, attains maximum and then decreases for further increase of wall distance.

5. The peak wall surface pressures on an inclined plate can exceed those on a perpendicular plate, the largest pressure being 7% above the normal impingement value. In the far field, the peak pressure increases as the wall inclination decreases and then decreases for further decrease in angle of inclination.

6. The quantitative visualization of the jet flow in the near field using Schlieren technique identifies Mach disks in the free jet zone and a bow shock convex upwards in the impingement zone.

REFERENCES

1. Donaldson, C.D. and Snedeker, R.S., "*A study of free jet impingement. Part 1. Mean properties of free and impinging jets*", Journal of Fluid Mechanics, vol 45, 1971, pp 281–319.

2. Gummer, J.H. and Hunt, B.L., *"The impingement of a uniform, axisymmetric, supersonic jet on a perpendicular flat plate"*, The Aeronautical Quarterly, vol 22, 1971, pp 403–420.

3. Bradbury, L.J.S., *"The impact of an axisymmetric jet onto a normal ground"*, The Aeronautical Quarterly, vol 23, 1972, pp 141–147.

4. Carling, J.C. and Hunt, B.L., *"The near wall jet of a normally impinging, uniform, axisymmetric, supersonic jet"*, Journal of Fluid Mechanics, vol 66, 1974, pp 159—176.

5. Pollard, D.J. and Bradbury, L.J.S., *"Impingement of a two-dimensional supersonic jet upon a normal ground surface"*, AIAA, vol14, 1976, pp 1095–1098.

6. Gutmark, E., Wolfshtein, M. and Wygnanski, I., *"The plane turbulent impinging jet"*, Journal of Fluid Mechanics, vol 88, 1978, pp 737–756.

7. Lamont, P.J. and Hunt B.L., *"The impingement of underexpanded, axisymmetric jets on perpendicular and inclined flat plates"* Journal of Fluid Mechanics, vol 100, 1980, pp 471–511.

8. Chich-ming Ho and Nagy, S., *"Dynamics of an impinging jet. Part 1. The feedback phenomenon"*, Journal of Fluid Mechanics, vol 105, 1981, pp 119–142.

9. Katok, K., Kamivama, Y., Hashimoto, S. and Komai, T., *"Mass transfer between a plane surface and an impinging turbulent jet: the influence of surface pressure fluctuations"*, Journal of Fluid Mechanics, vol 119, 1982, pp 91–105.

10. Hwang Jack, C., Tsou, F.K. and Woncheol C. Chou, *"K-E computations of flow and heat transfer in plane oblique impinging jets"*, Proceedings of the International conference, Washington, 1982, pp 271–282.

11. Looney, M.K. and Walsh, J.J., *"Mean-flow and turbulent characteristics of free and impinging jet flows"*, Journal of Fluid Mechanics, vol 147, 1984, pp 397–429.

12. Iwamoto, J., *"Impingement of underexpanded jets on a flat plate"*, Journal of Fluids Engineering, vol 112, 1990, pp 179–184.

13. Rajarathnam, N., *"Turbulent jets (Development in water science; 5)"*, Elsevier Scientific Publishing Company, Amsterdam, 1976.

14. Ricou, F.P. and Spalding D.B., *"Measurements of entrainment by axisymmetrical turbulent jets"*,Journal of Fluid Mechanics, vol 11, 1961, pp 21–32.

15. Nagy S. Nosseir, *"Impinging jets"*, Encyclopedia of Fluid Mechanics, vol 2, 1986, pp 349–366.

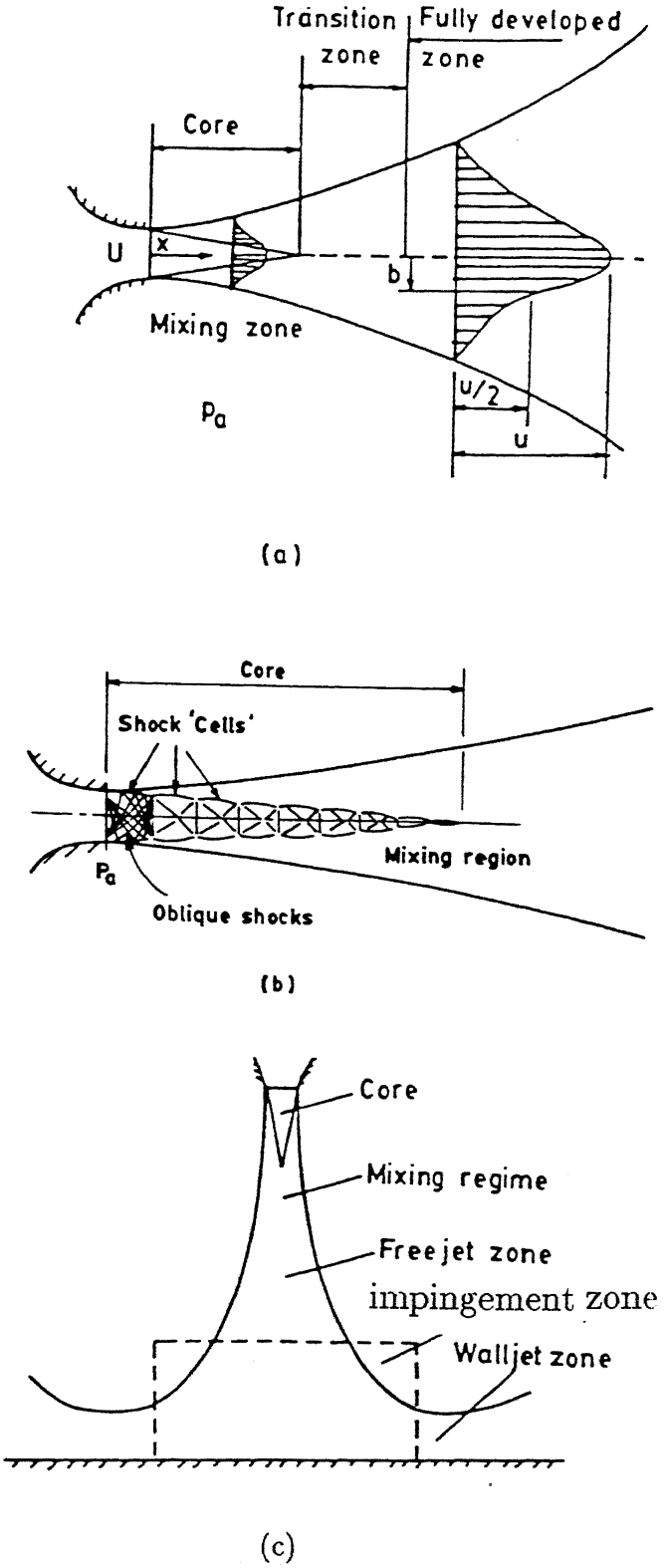

Figure 1. General features of jet flow. a) subsonic free jet
b) moderately underexpanded free jet c) impinging jet

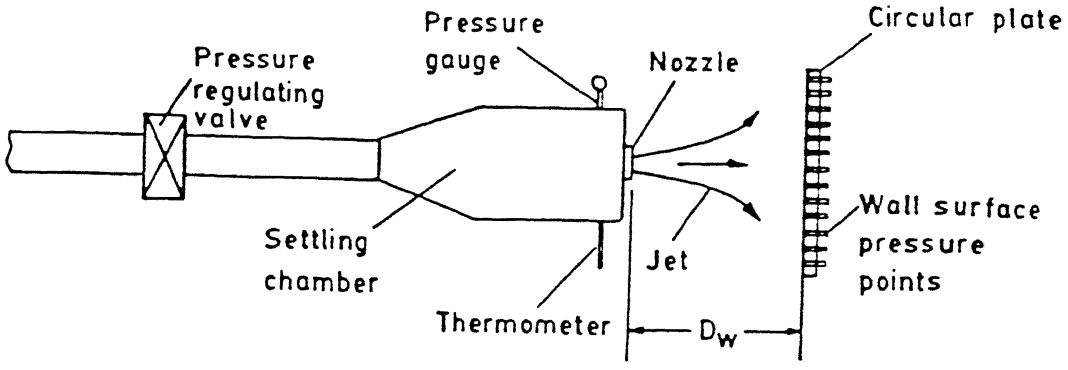

Figure 2a. Schematic of the internal flow facility.

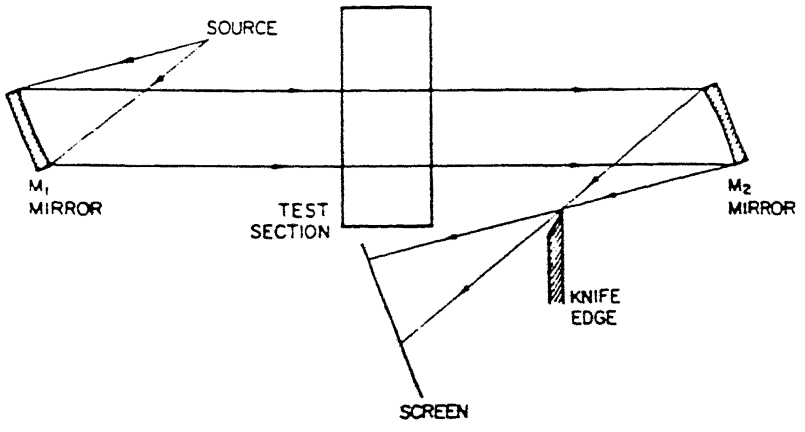

Figure 2b. Experimental arrangement for Schlieren system.

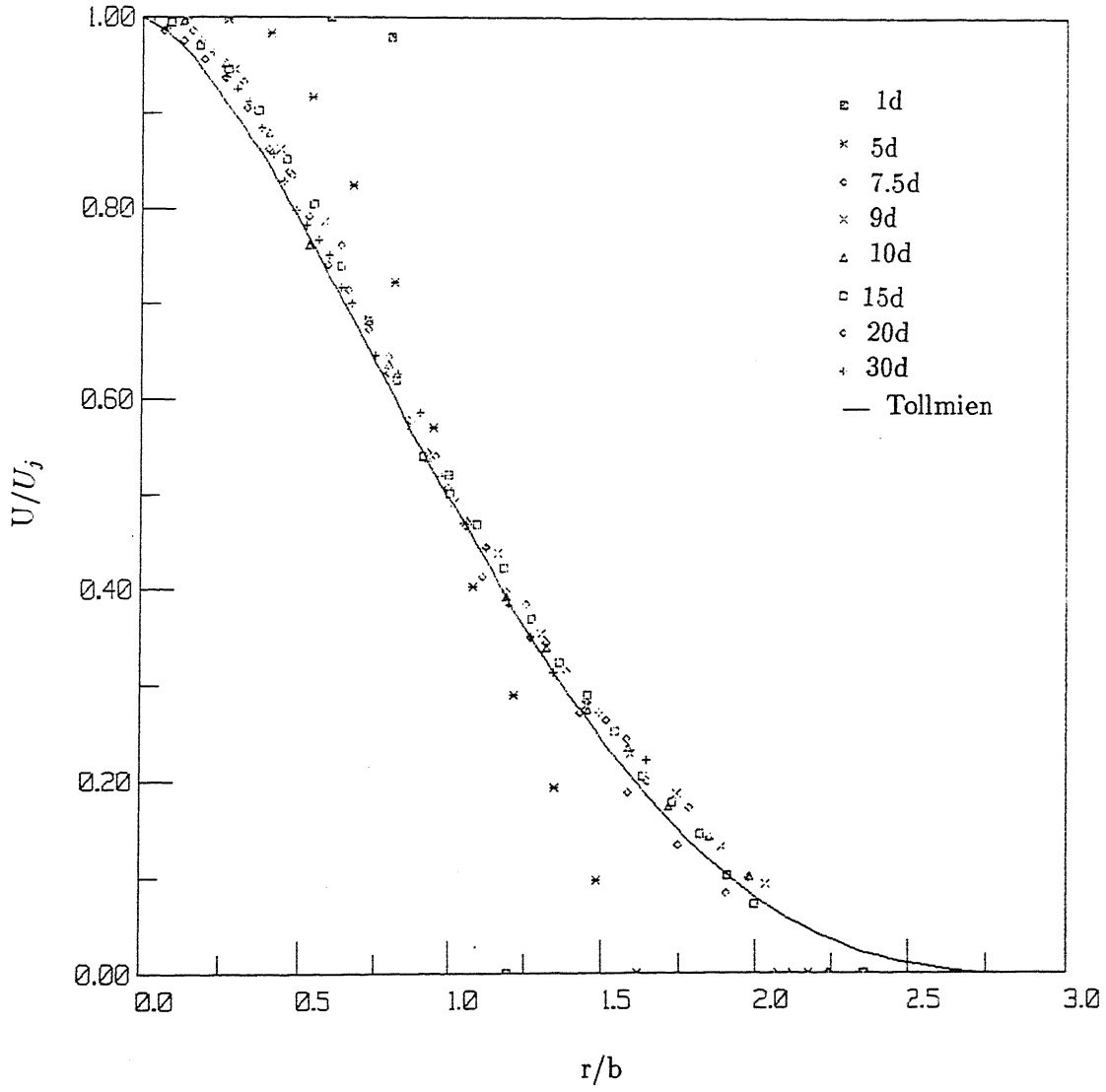

Figure 3. Mean velocity profiles of free jet for M_e=0.8.

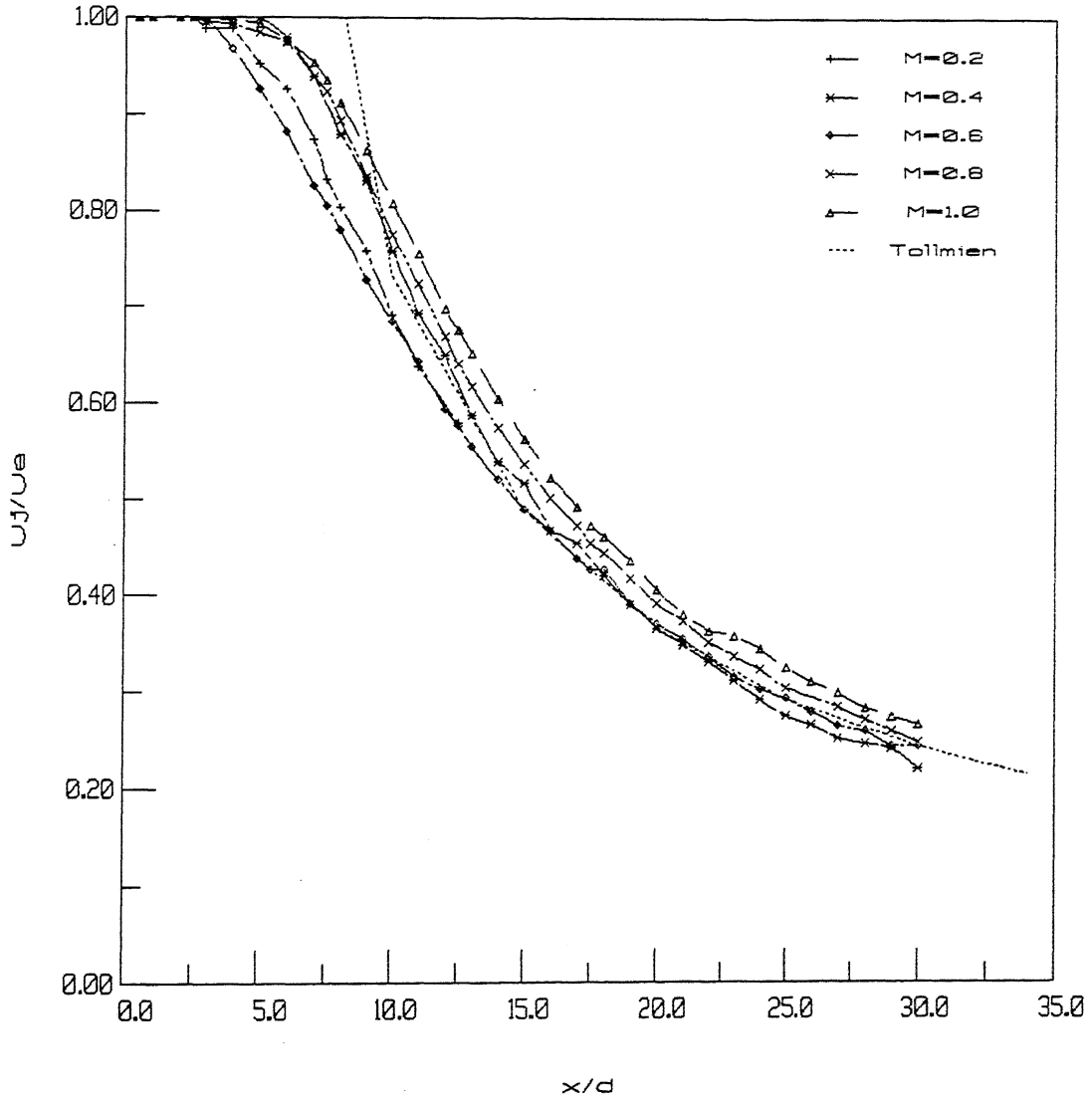

Figure 4. Axial velocity decay of freejet.

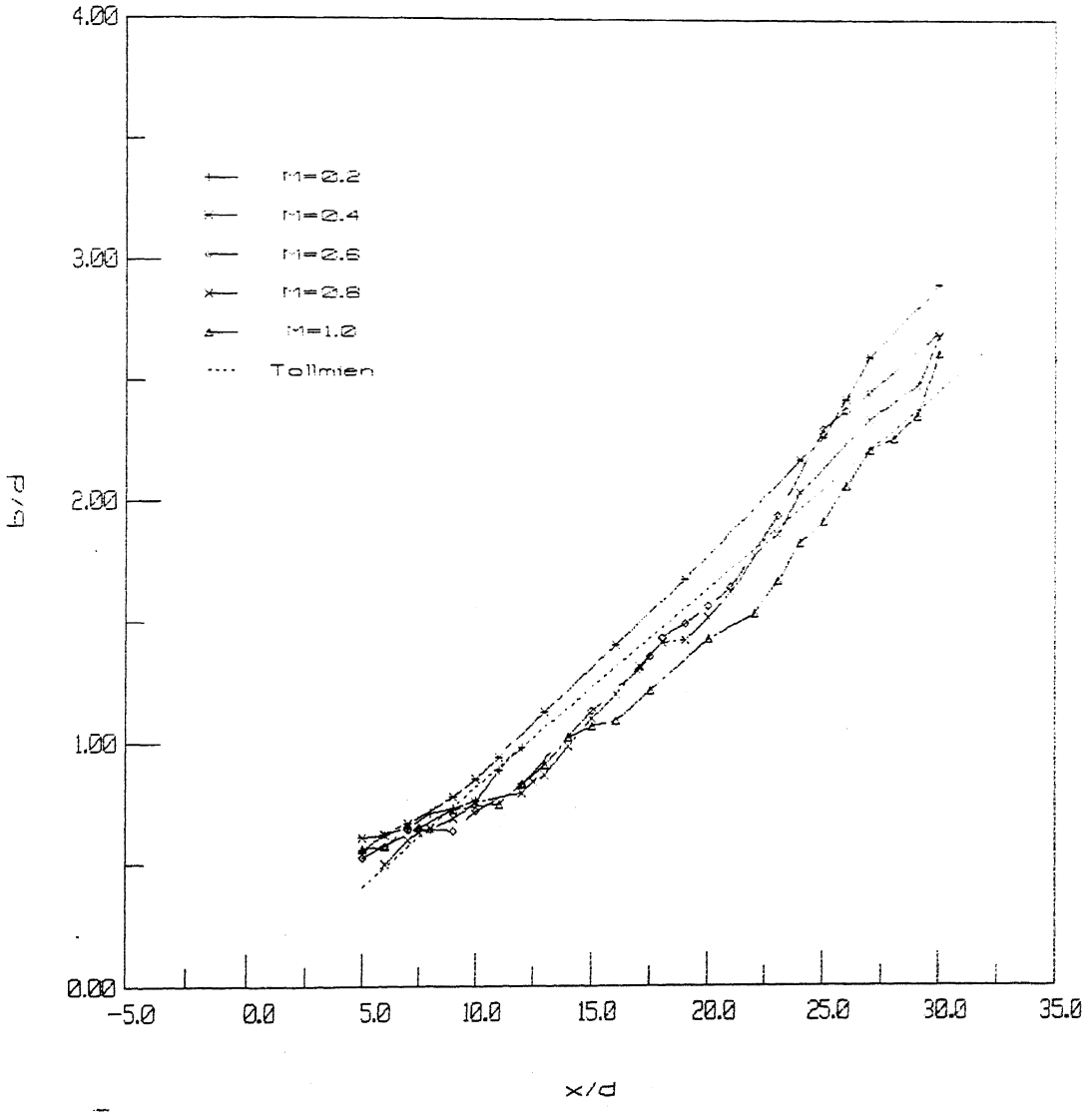

Figure 5. Variation of spread width of freejet along the axis.

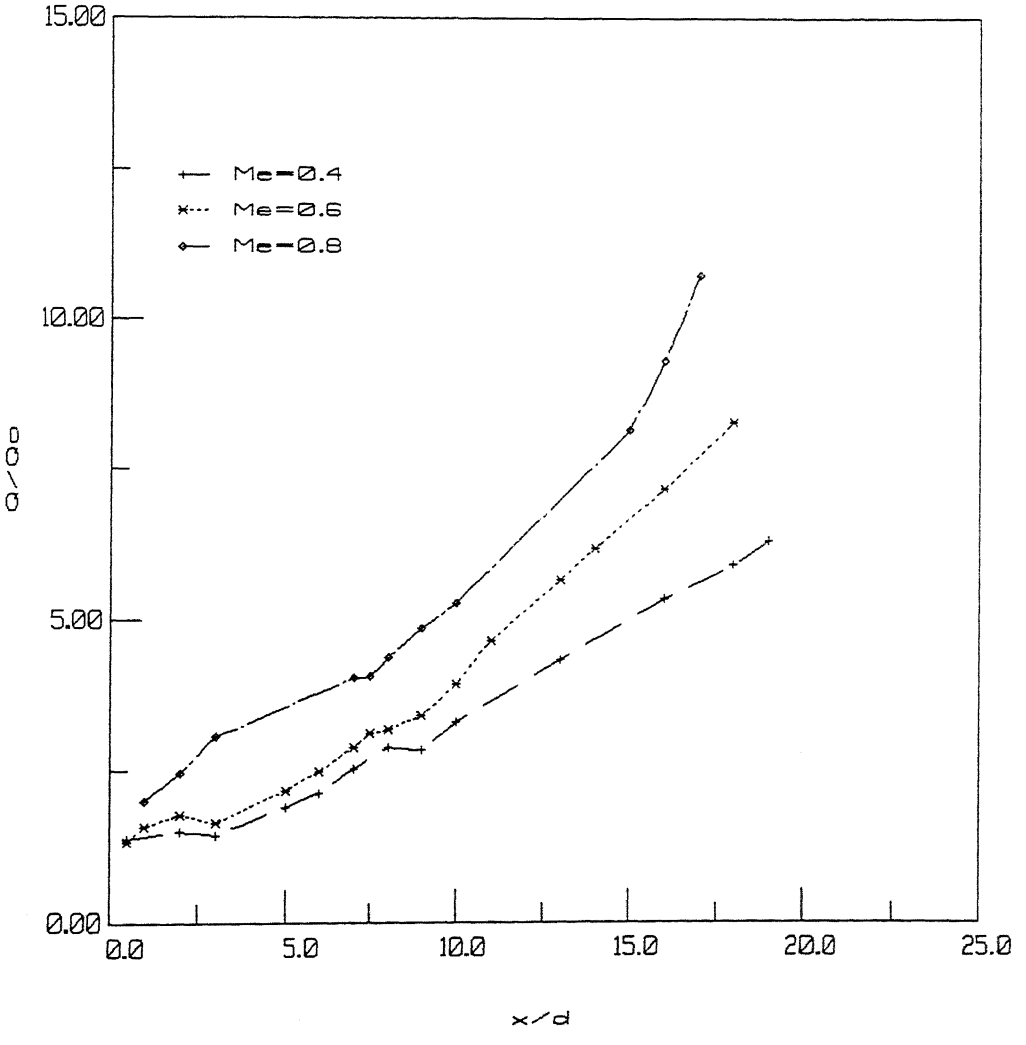

Figure 6. Entrainment of freejet.

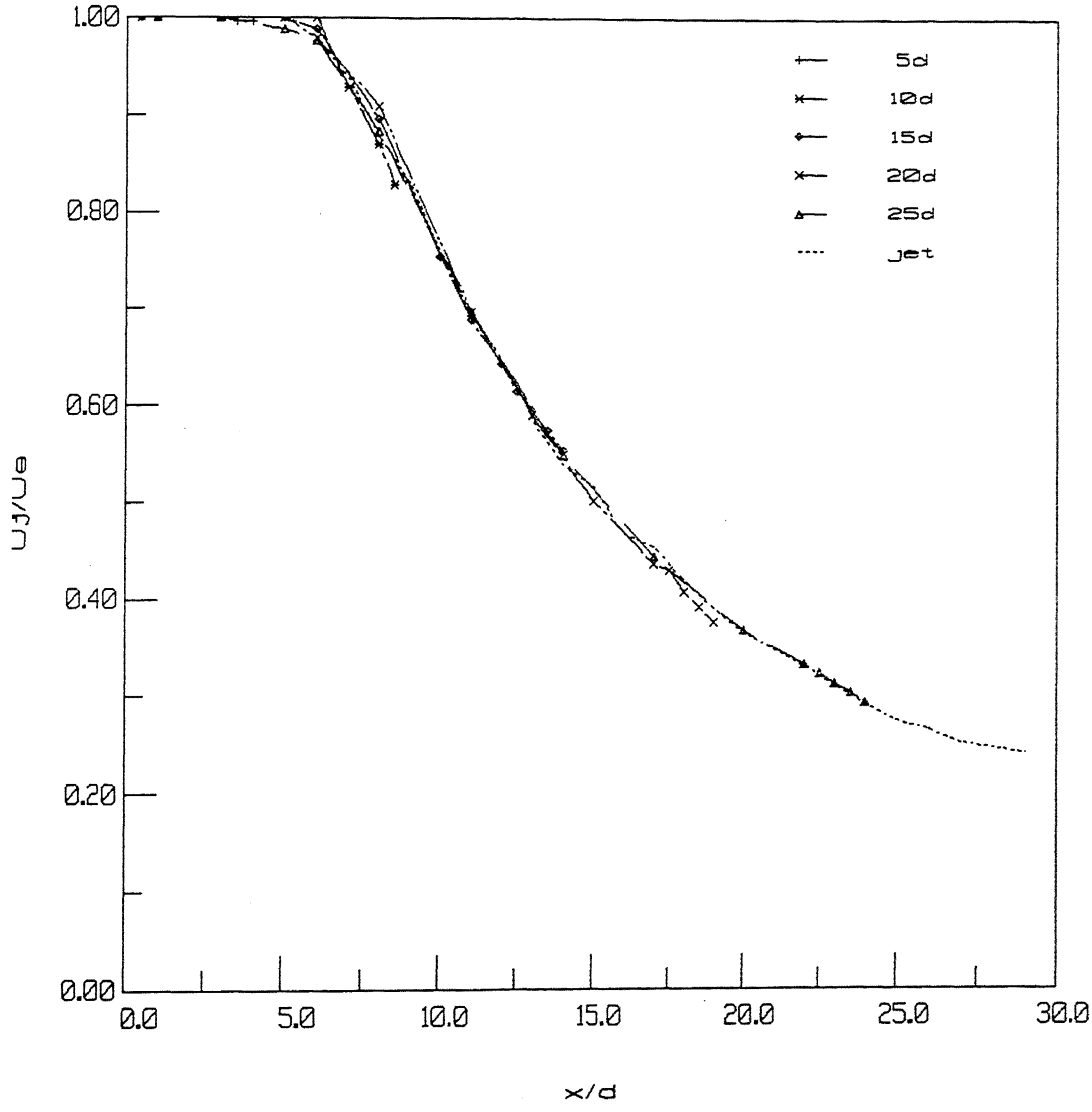

Figure 7. Axial velocity decay of impinging jet for Me=0.4.

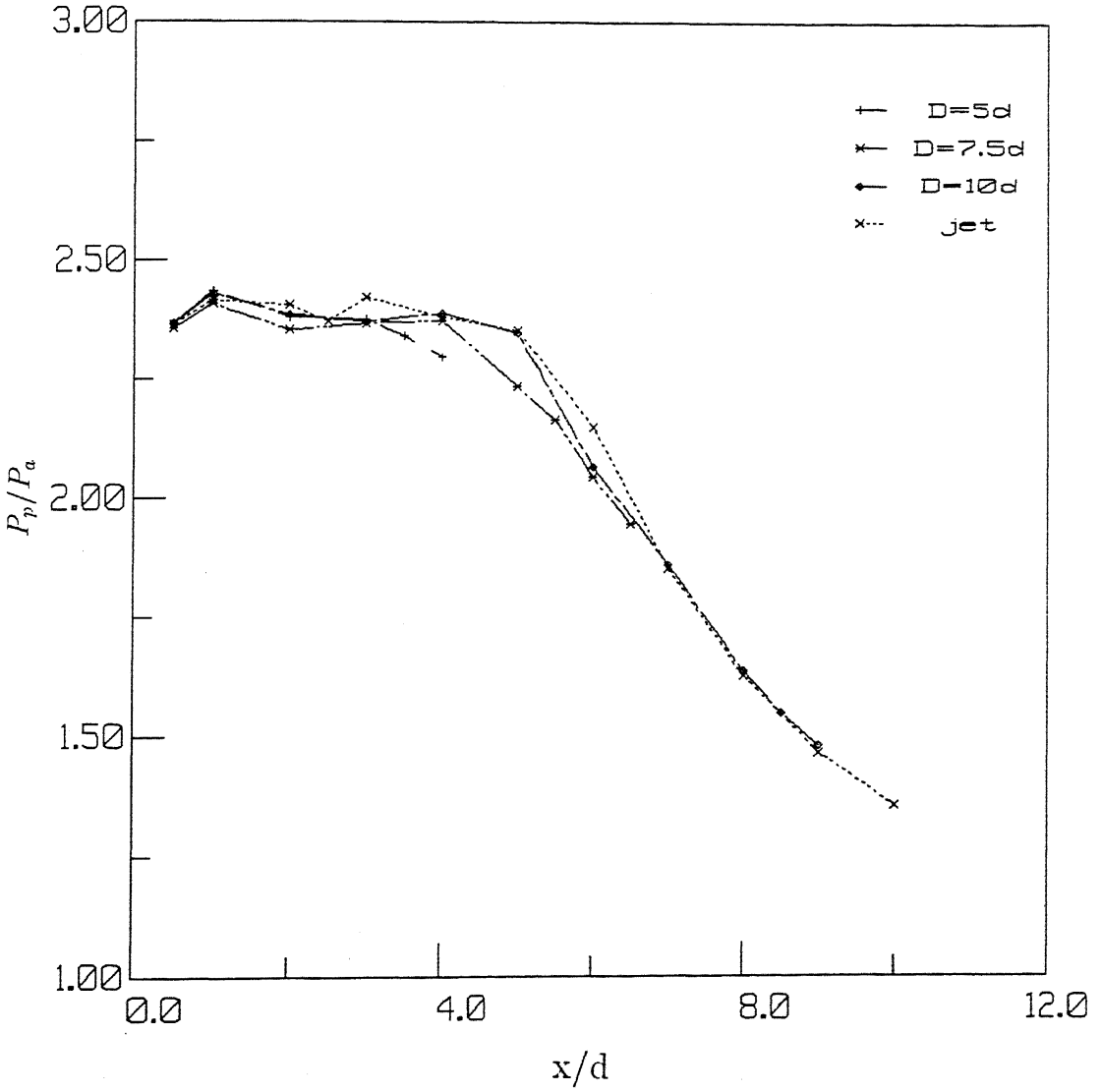

Figure 8. Axial decay of pitot pressure of impinging jet for underexpanded flow.

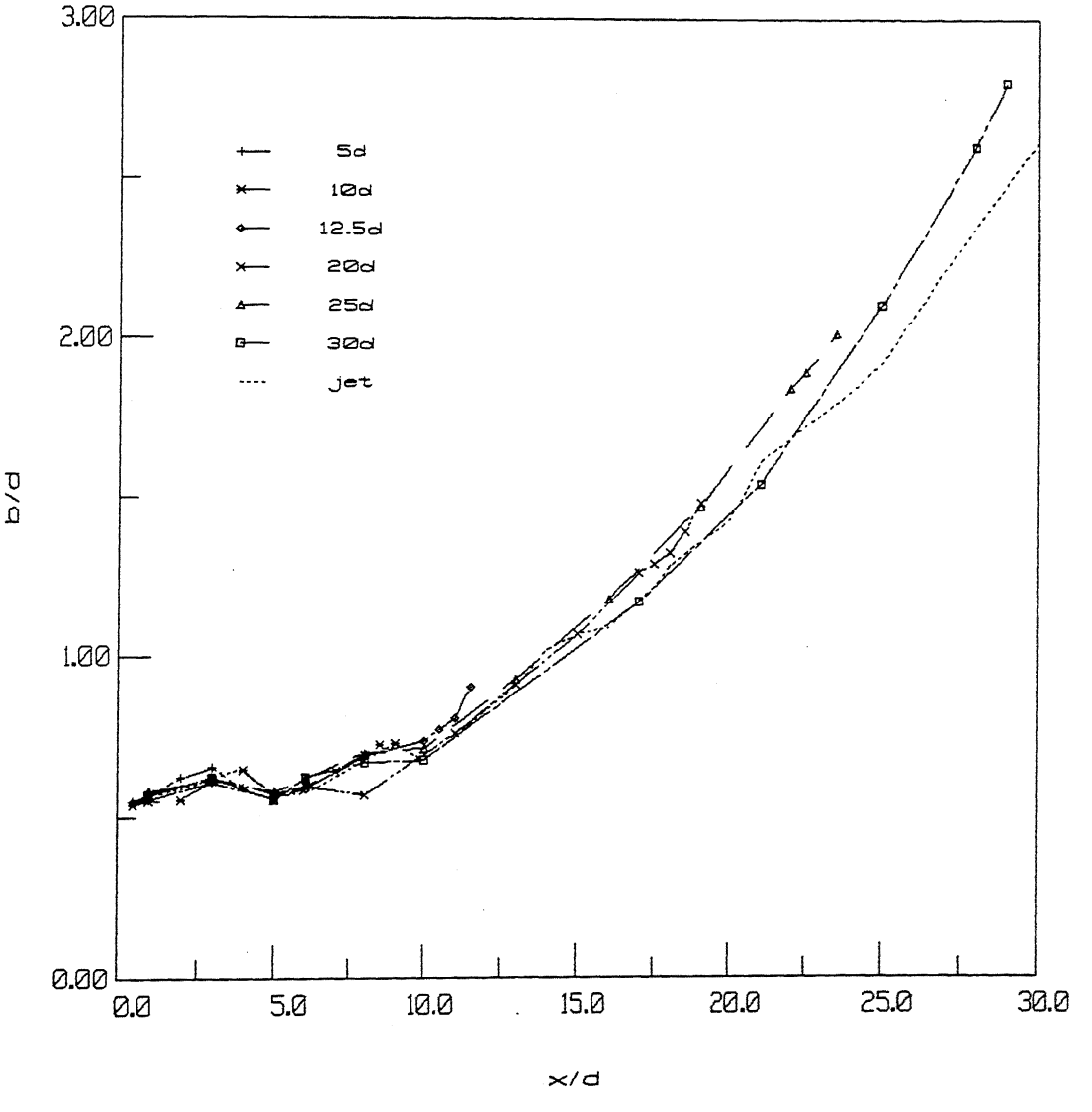

Figure 9. Measured spread of impinging jet along the axis for Me=1.0.

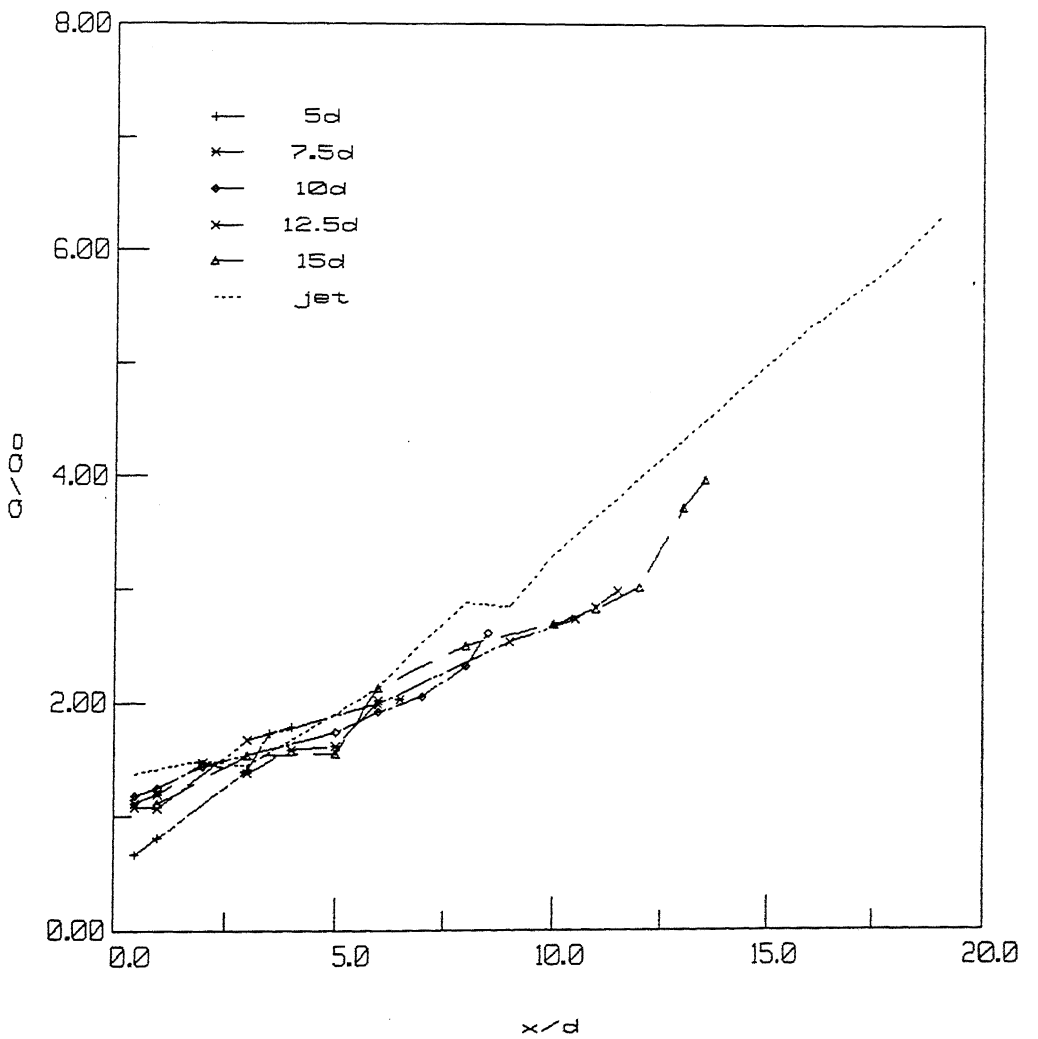

Figure 10. Entrainment of impinging jet for Me=0.4.

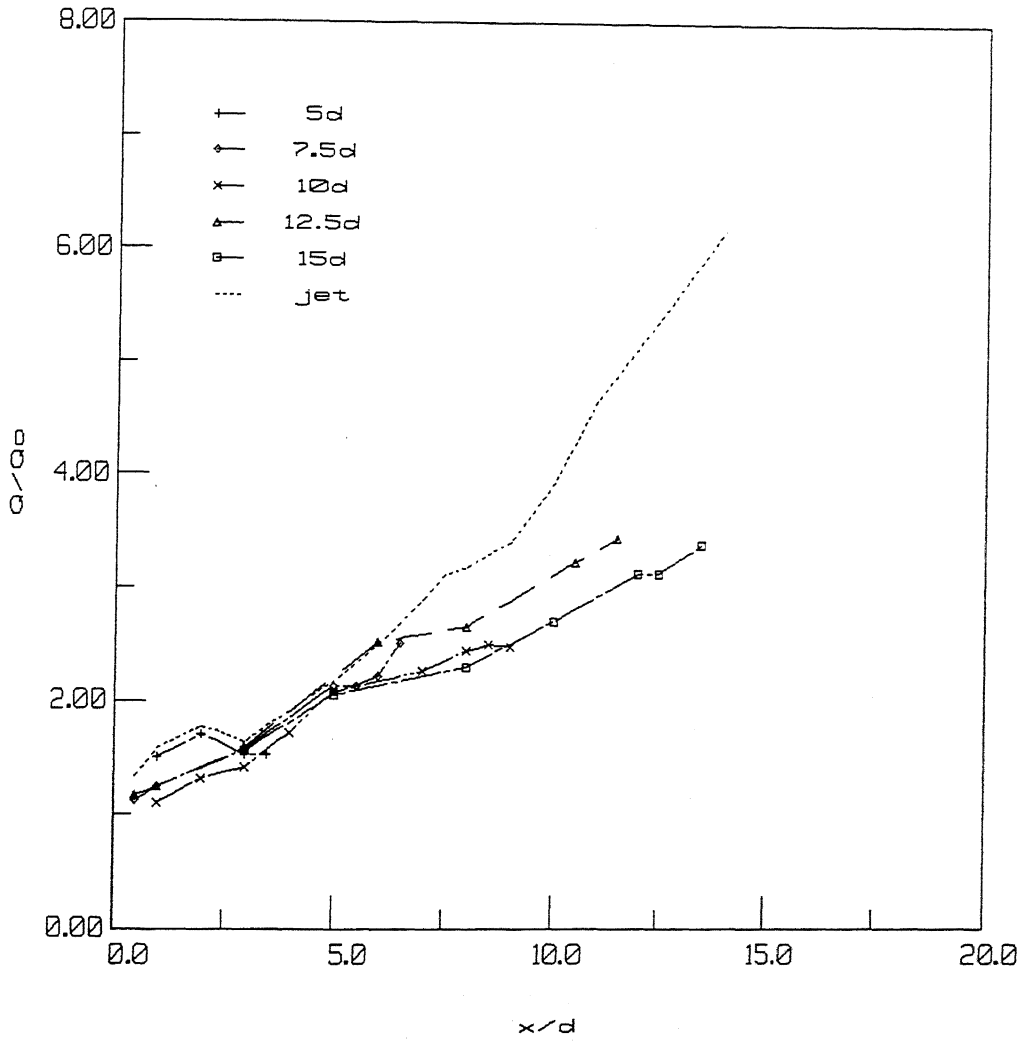

Figure 11. Entrainment of impinging jet for Me=0.6.

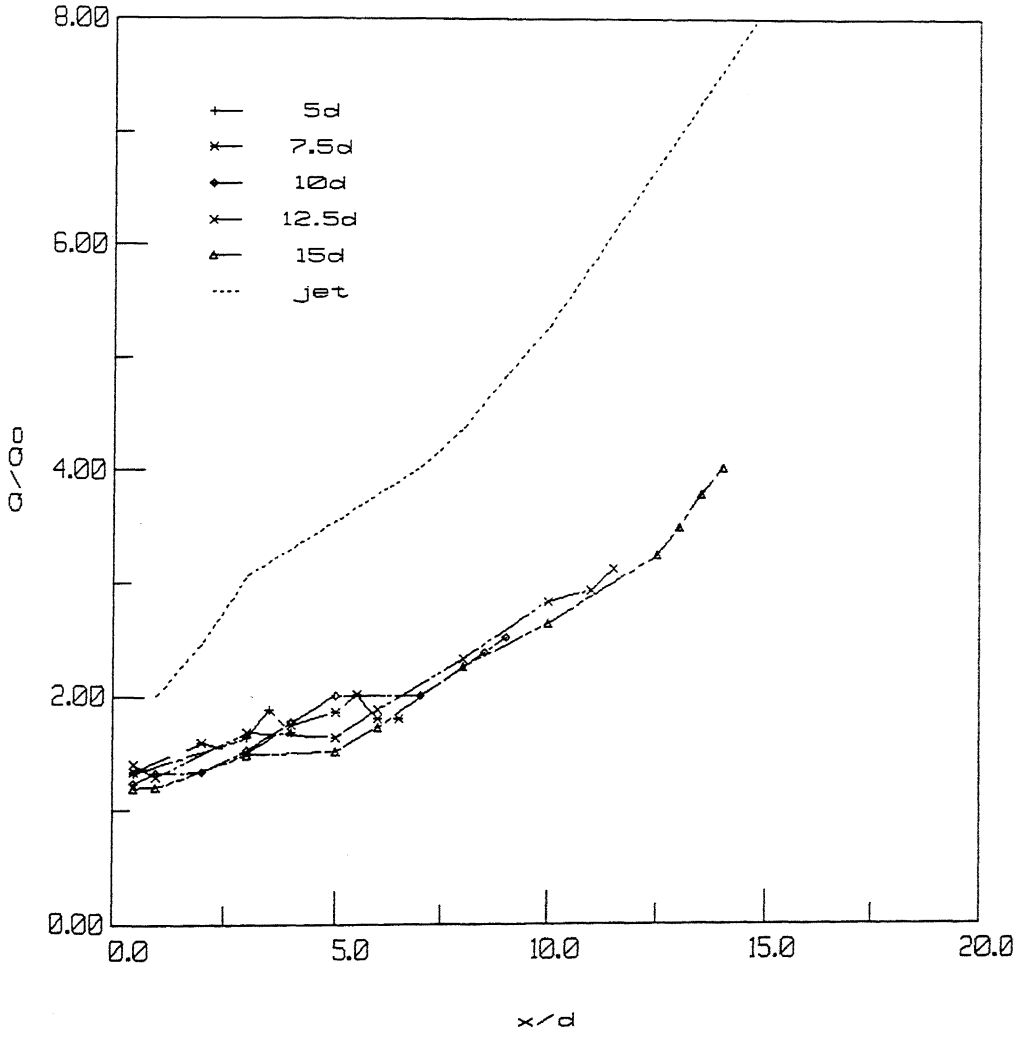

Figure 12. Entrainment of impinging jet for Me=0.8.

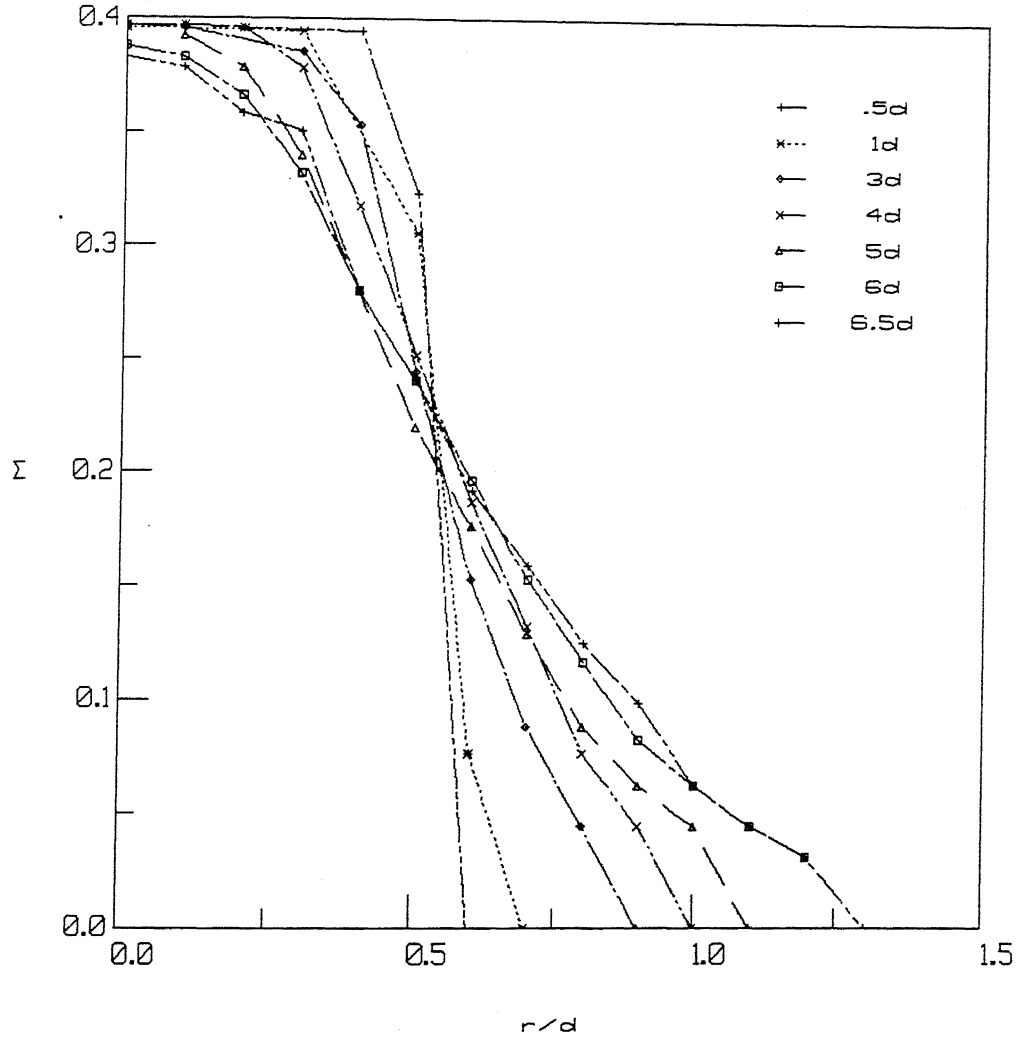

Figure 13. Mach number variation of impinging jet for Me=0.4 and Dw=7.5d.

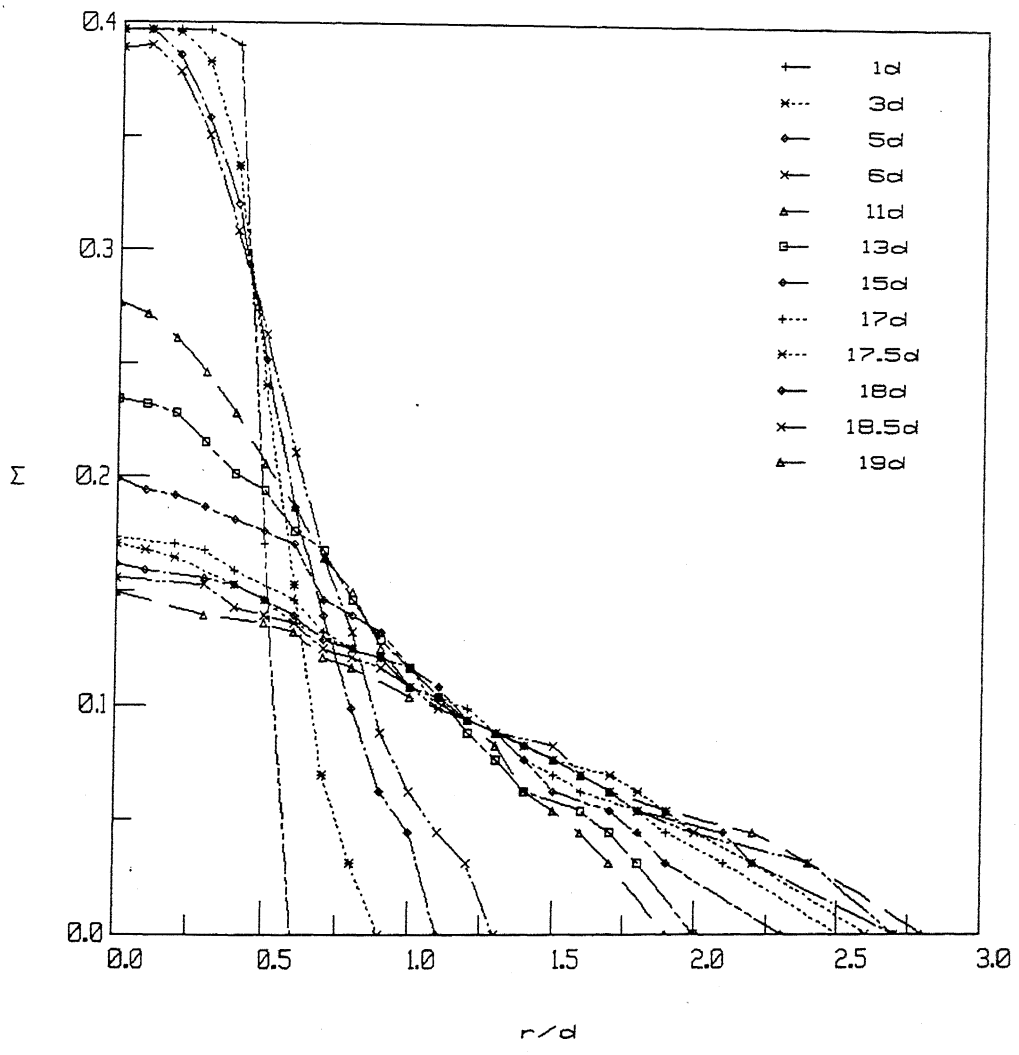

Figure 14. Mach number variation of impinging jet for Me=0.4 and Dw=20d.

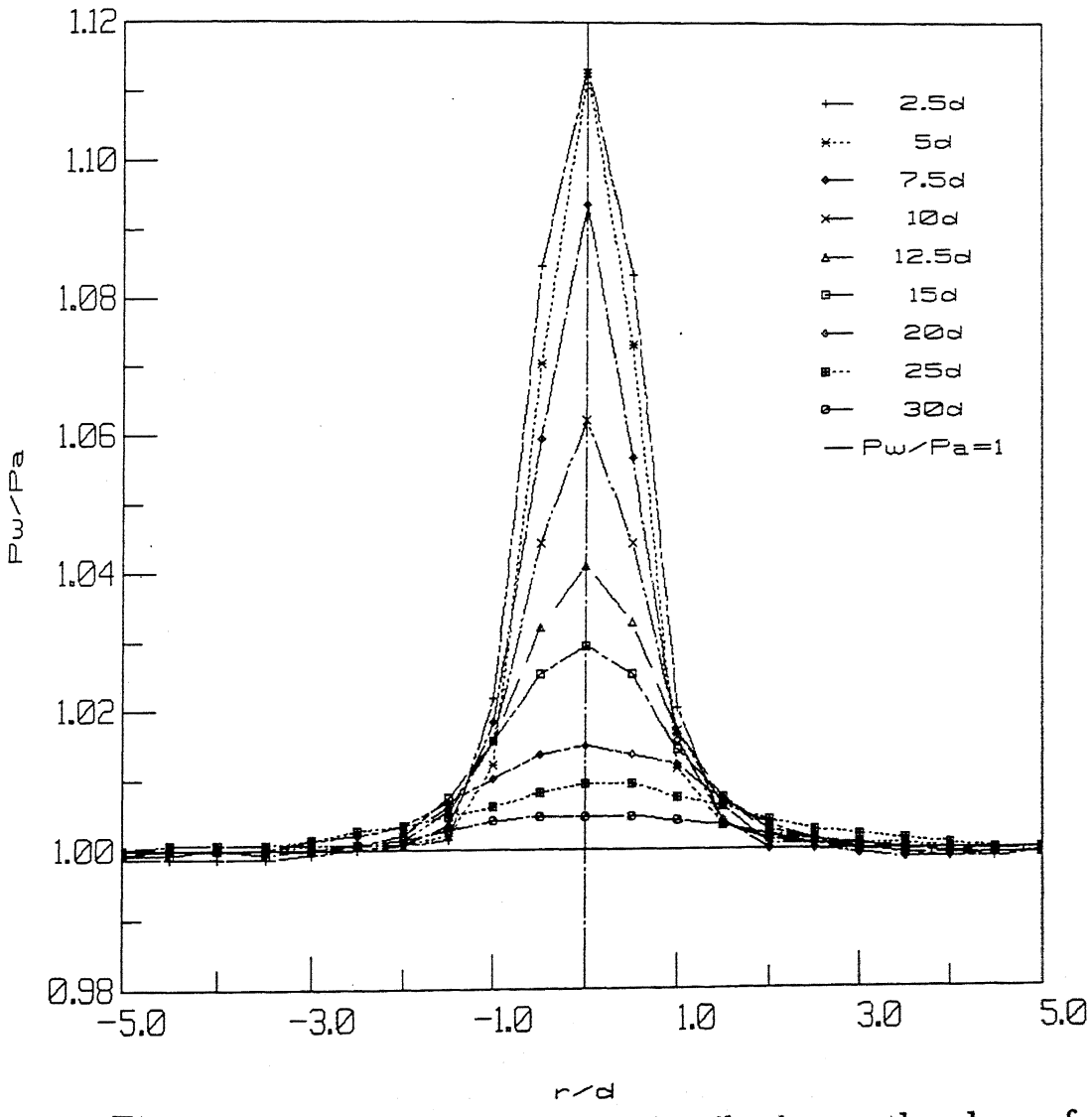

Figure 15. Wall surface pressure distribution on the plane of symmetry for Me=0.4.

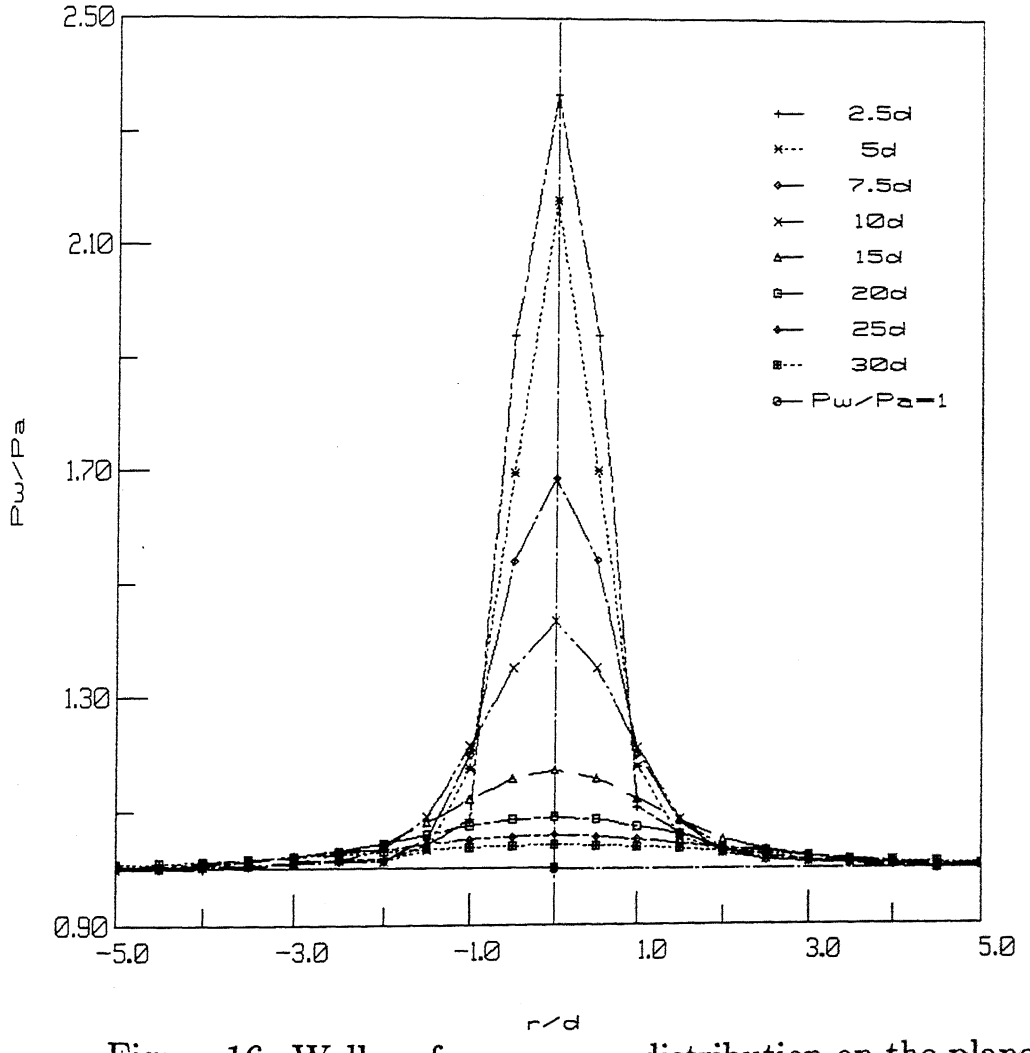

Figure 16. Wall surface pressure distribution on the plane of symmetry for underexpanded flow.

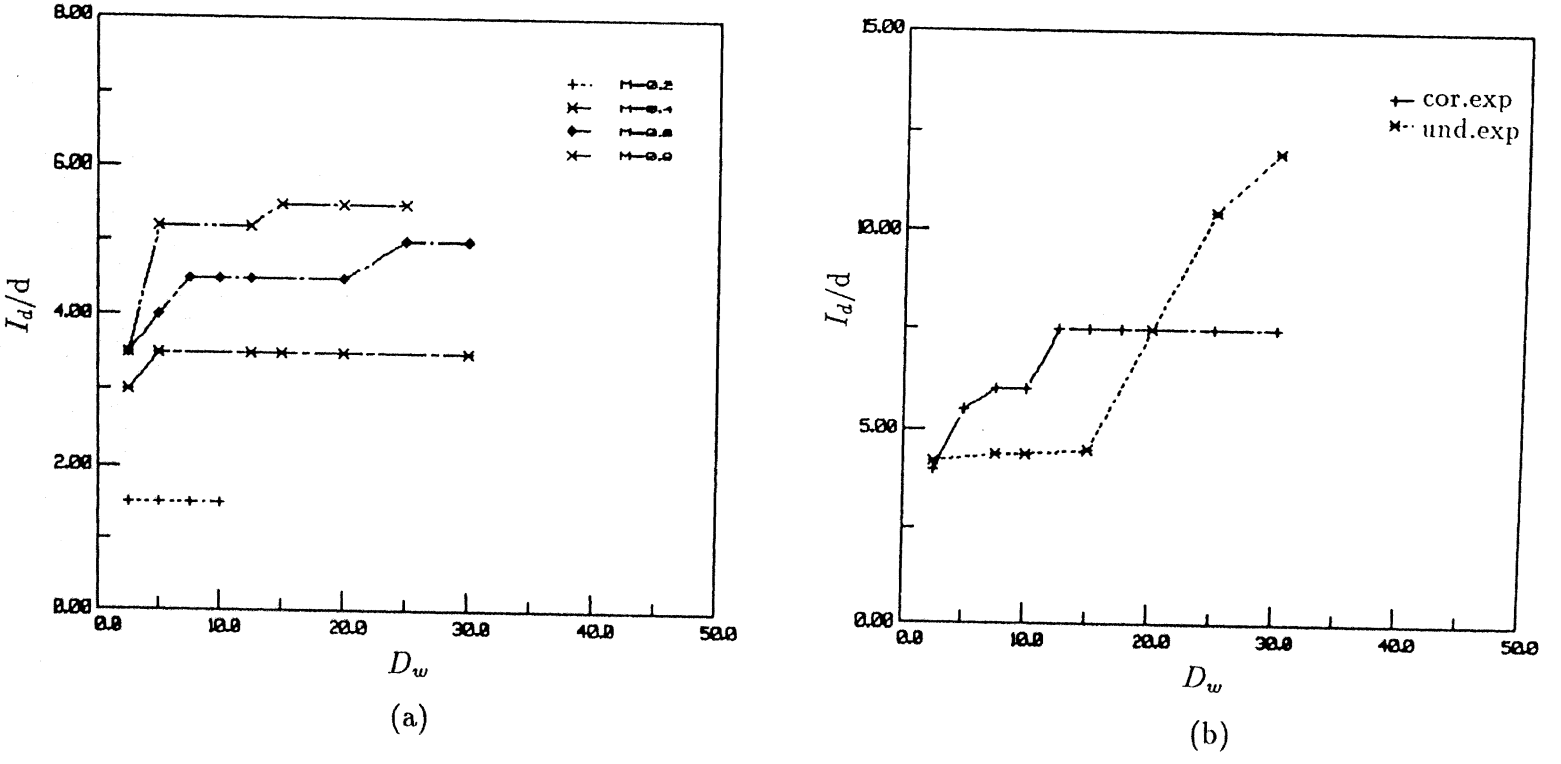

Figure 17. Variation of influence zone with wall distance.
a) for subsonic jets b) sonic and underexpanded jets

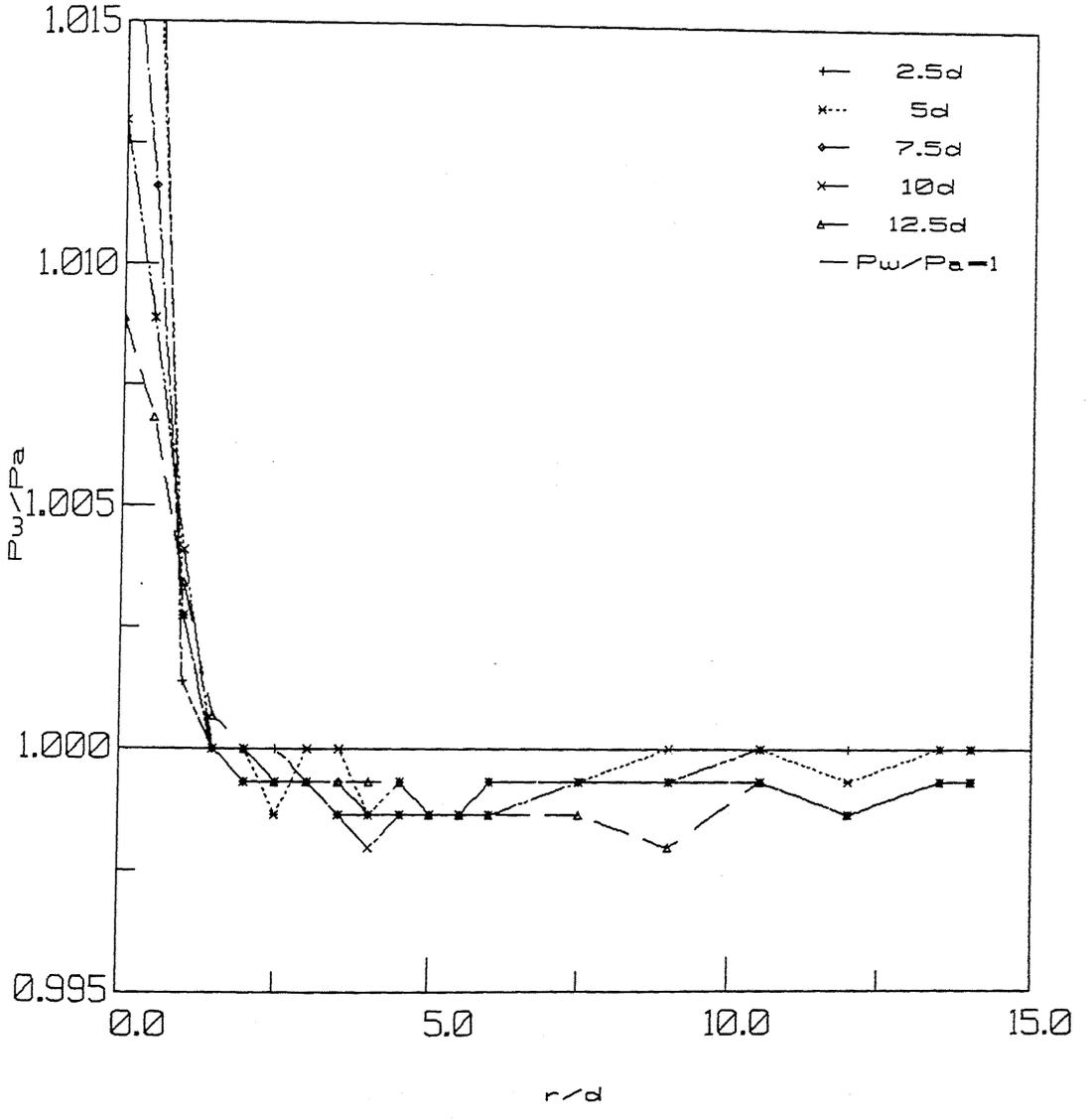

Figure 18. Wall surface pressure distribution for Me=0.2.

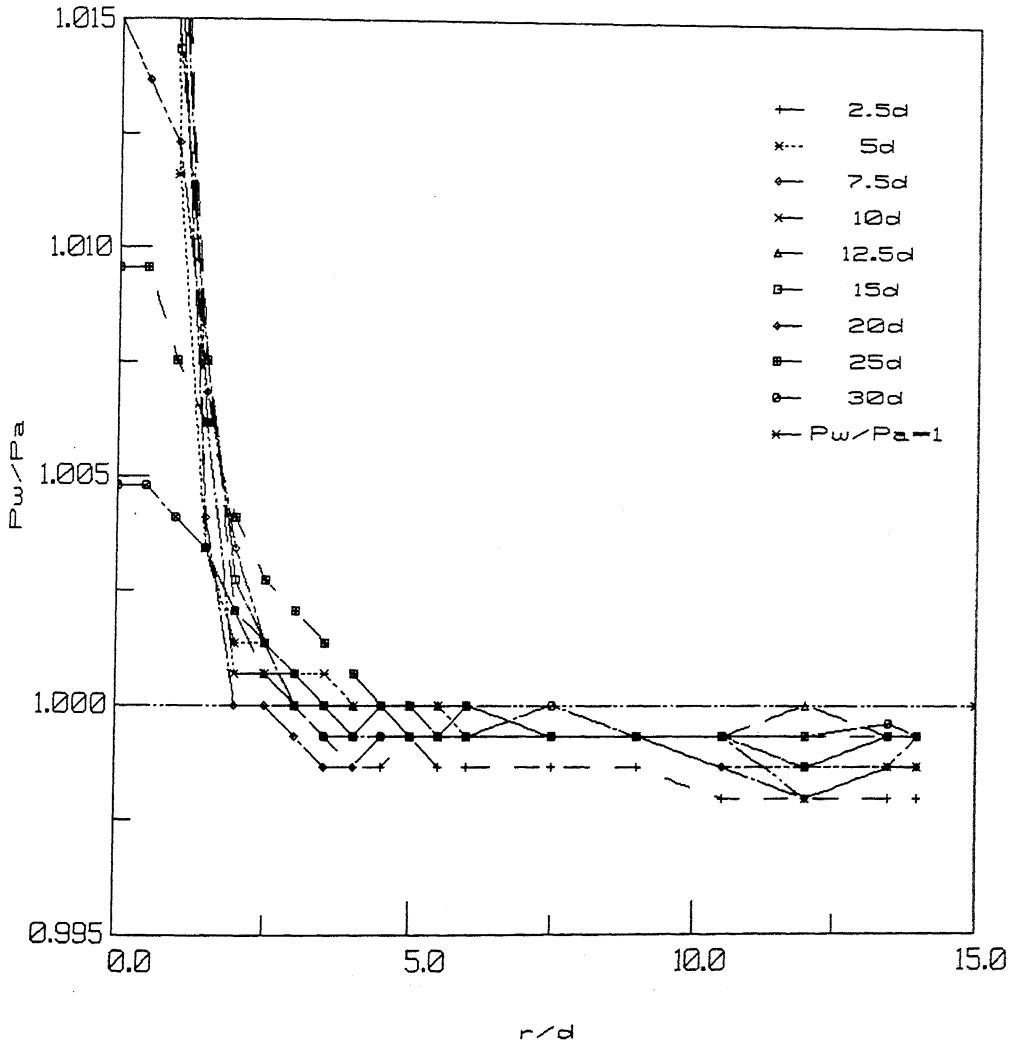

Figure 19. Wall surface pressure distribution for Me=0.4.

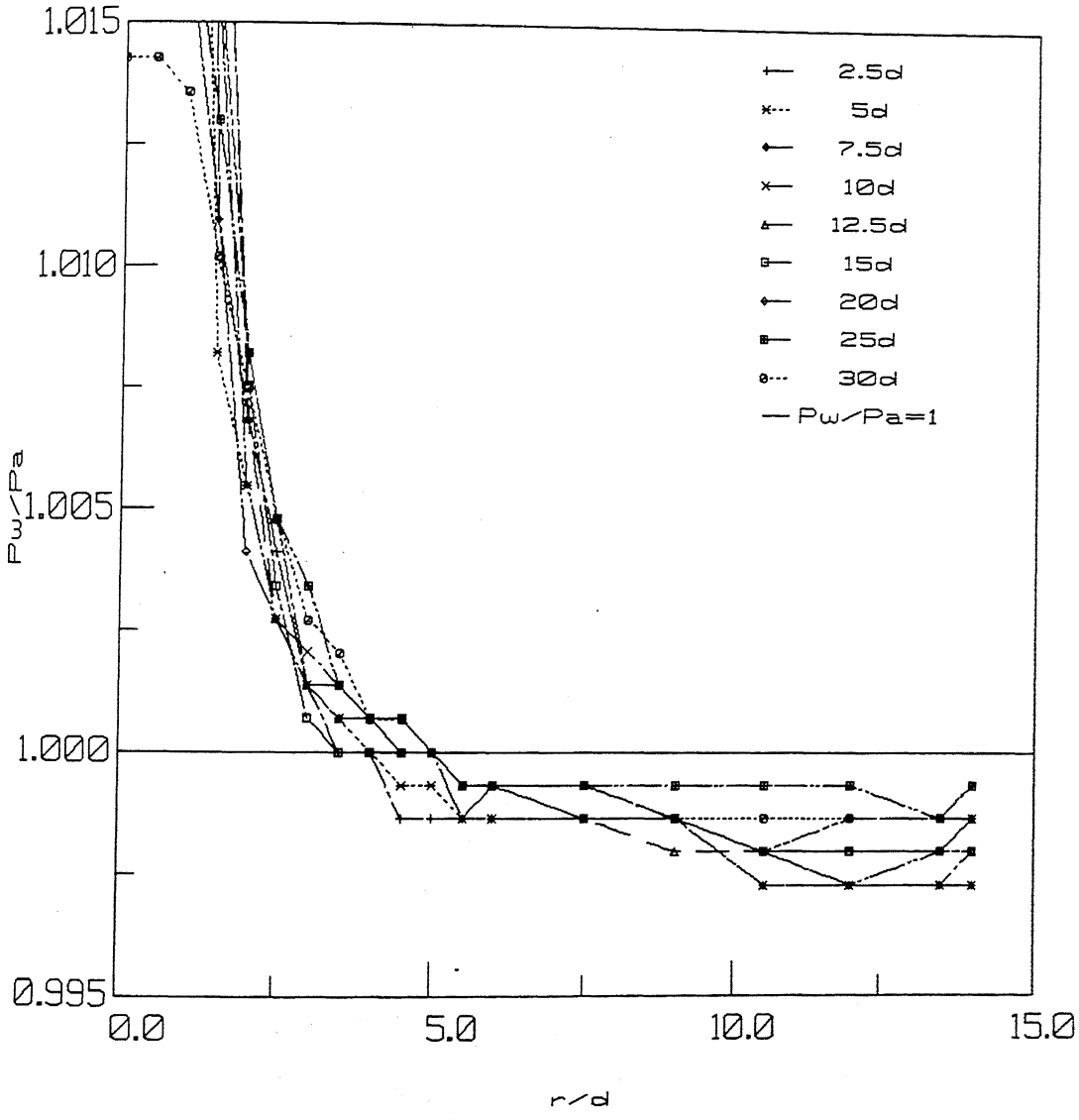

Figure 20. Wall surface pressure distribution for Me=0.6.

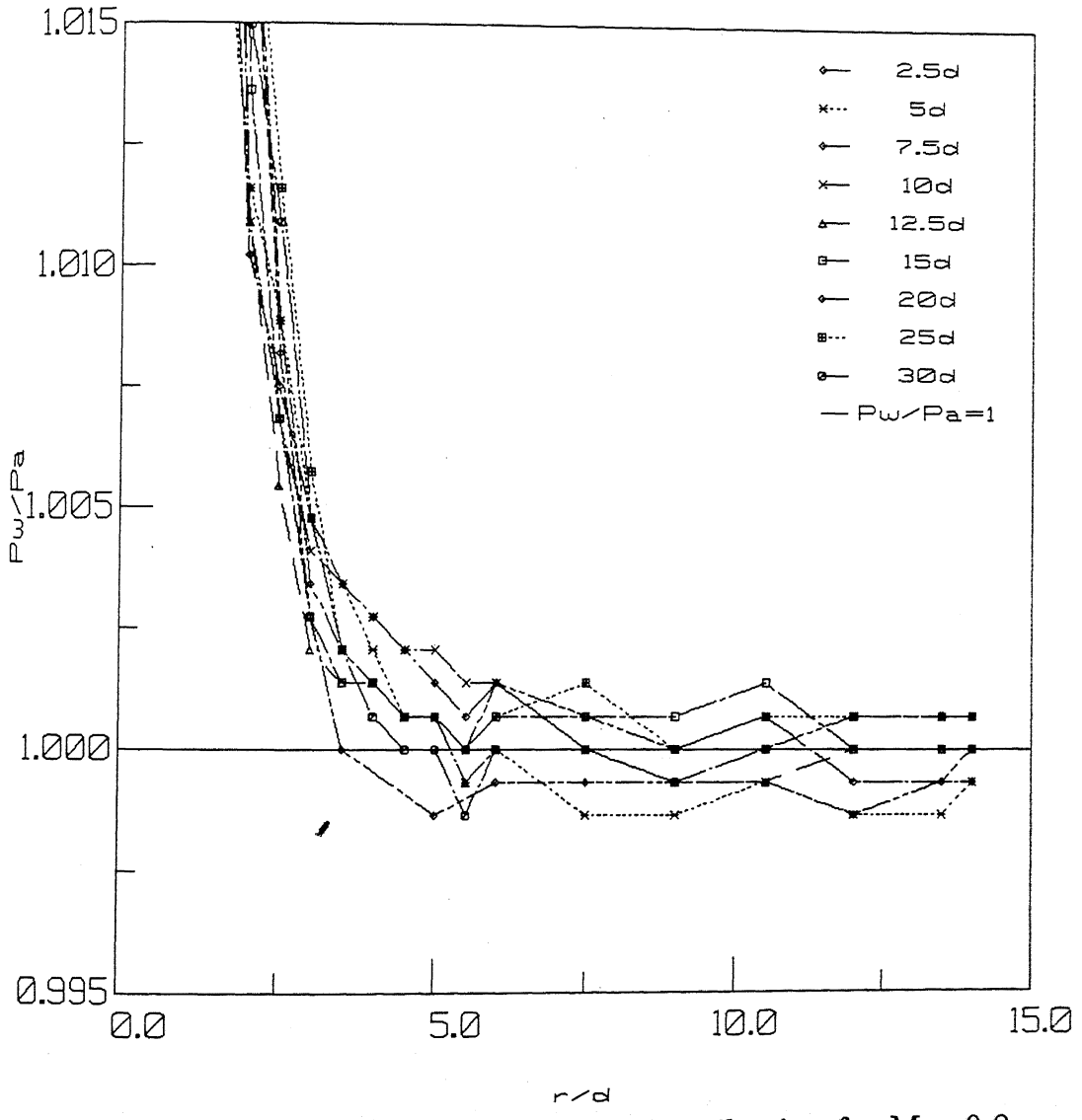

Figure 21. Wall surface pressure distribution for Me=0.8.

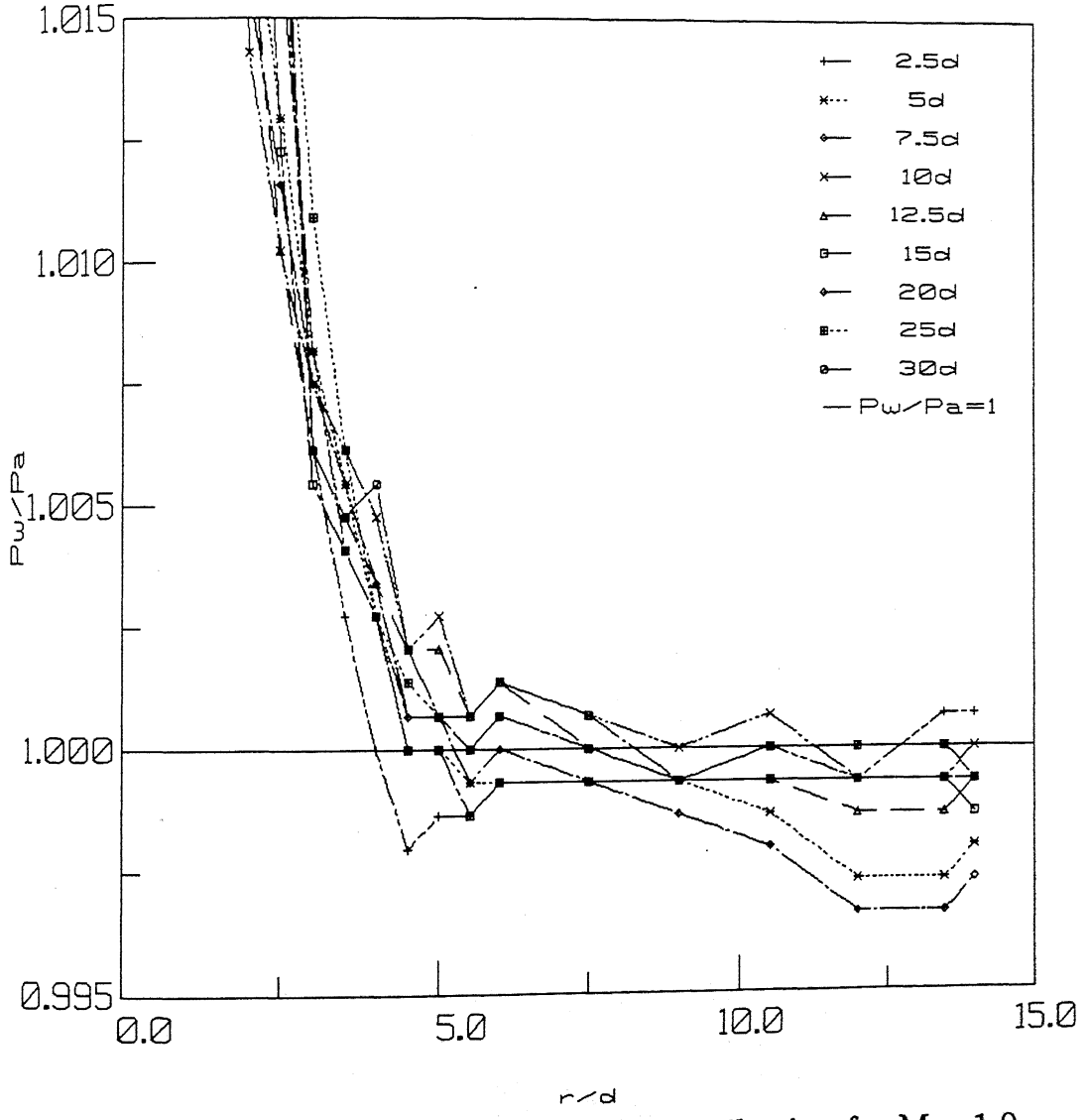

Figure 22. Wall surface pressure distribution for Me=1.0.

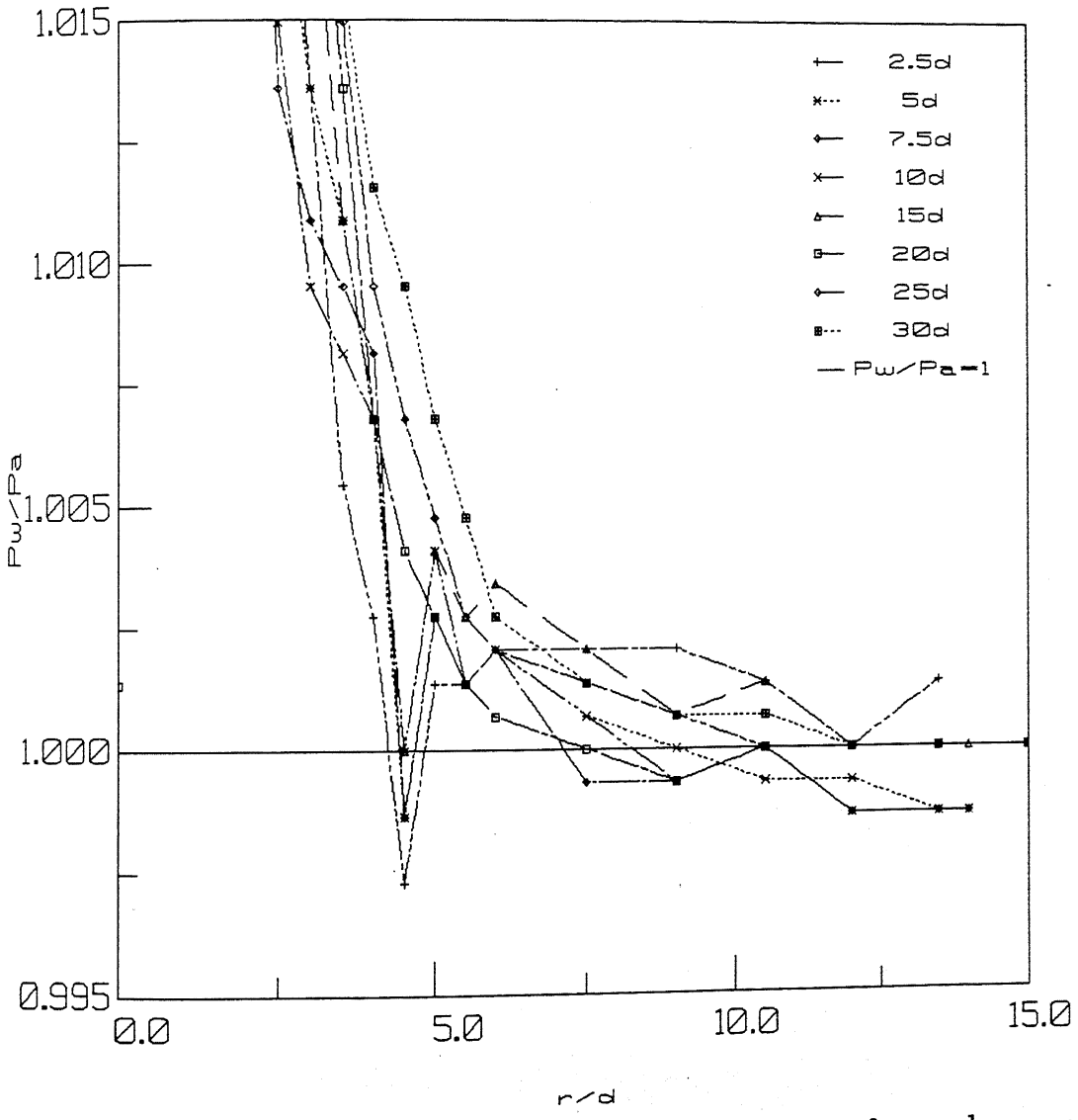

Figure 23. Wall surface pressure distribution for underexpanded flow.

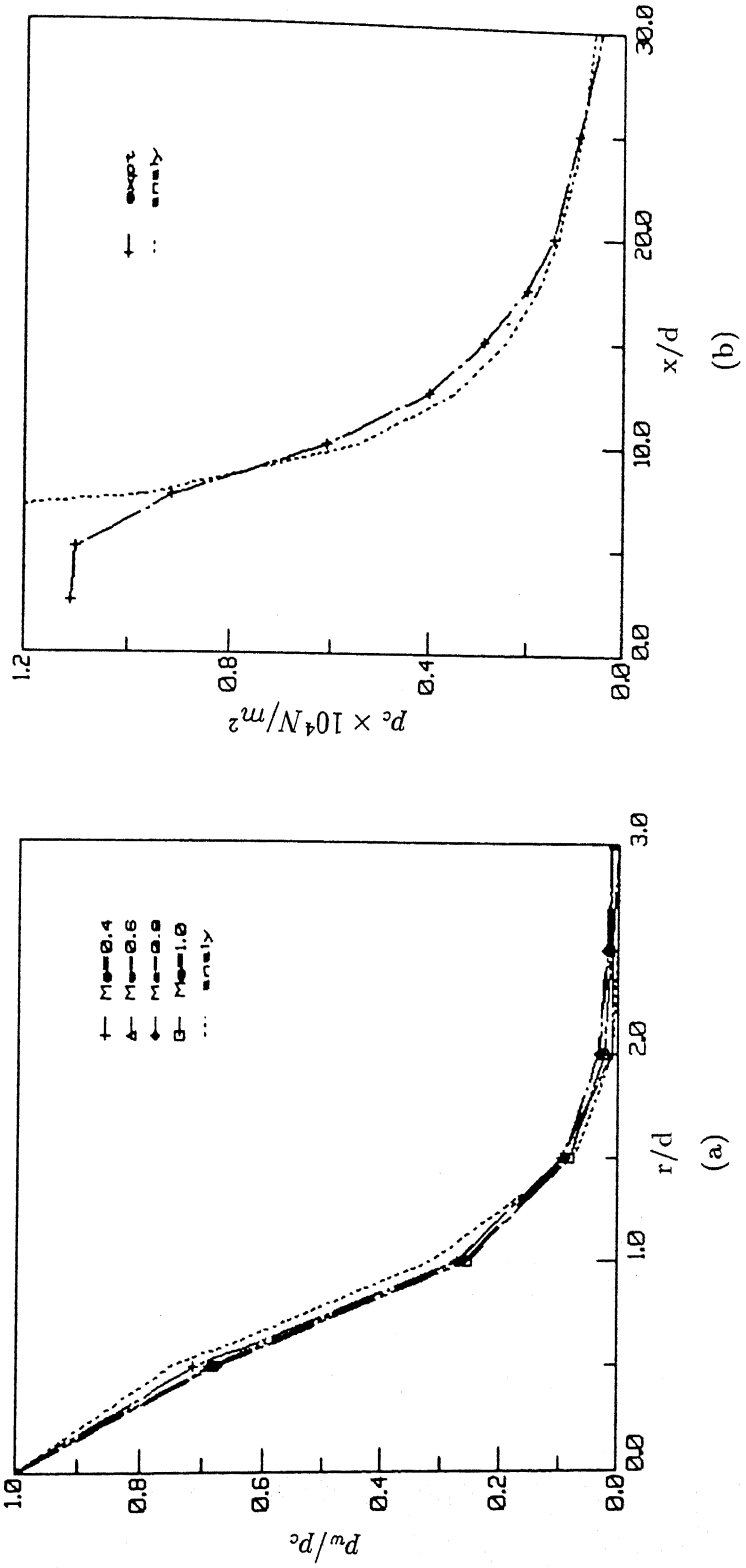

Figure 24. Comparison of wall surface pressure distribution with theory.
a) radial variation b) axial variation for Me=0.4.

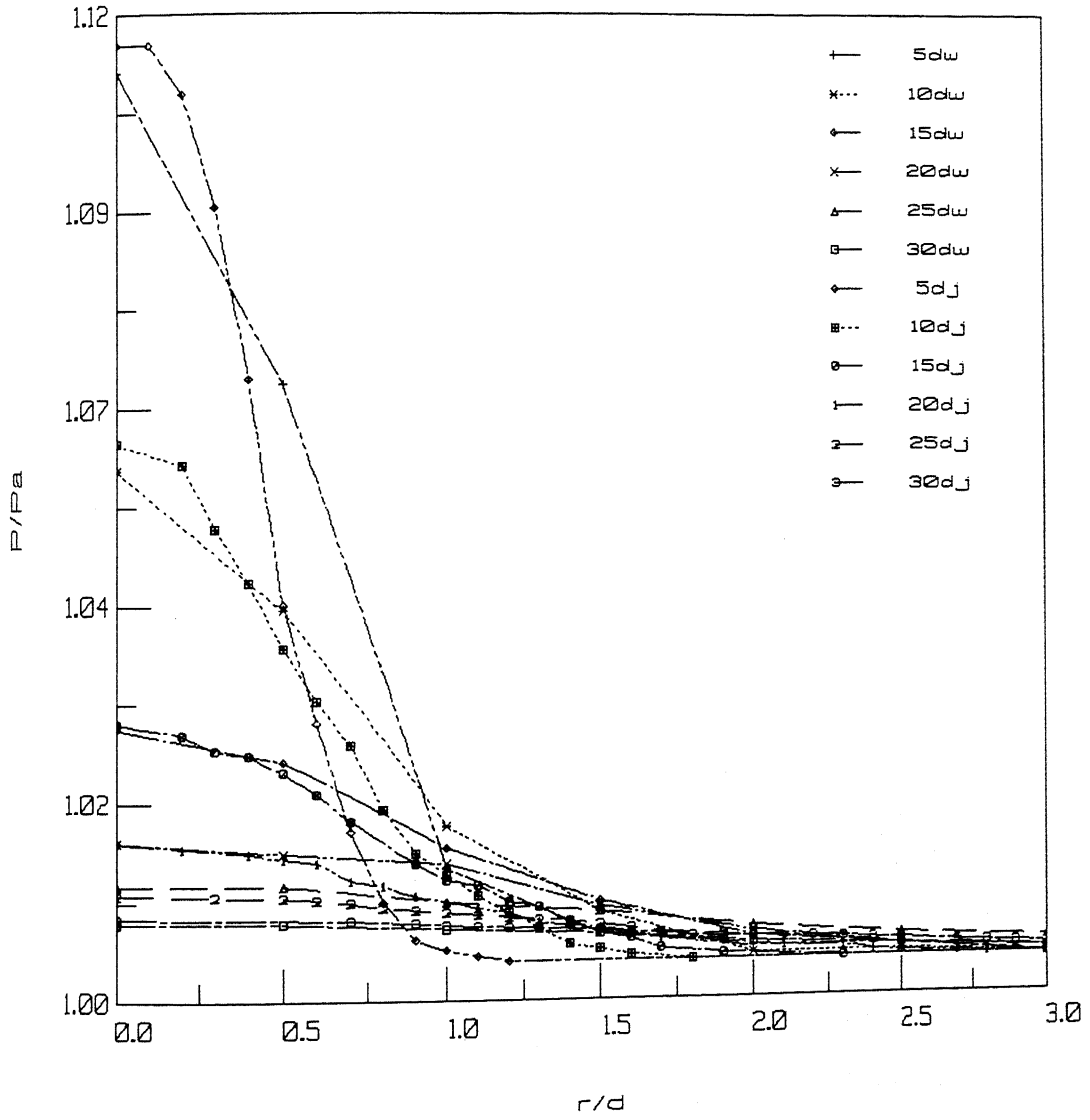

Figure 25. Comparison of freejet and wall surface pressures for Me=0.4. (d_j – free jet and d_w – wall axial locations).

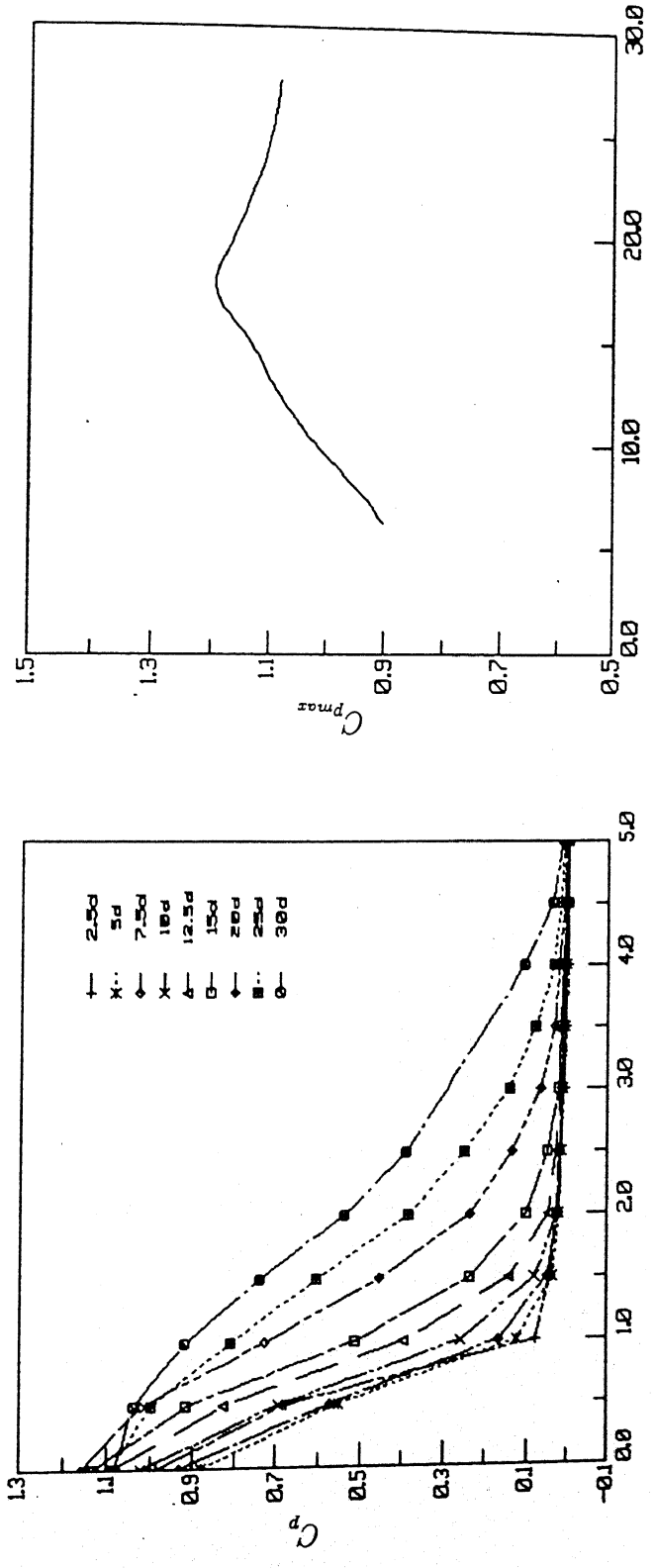

Figure 26. The intensity of impingement correlated with freejet data for Me=1.0. a) radial variation b) axial variation

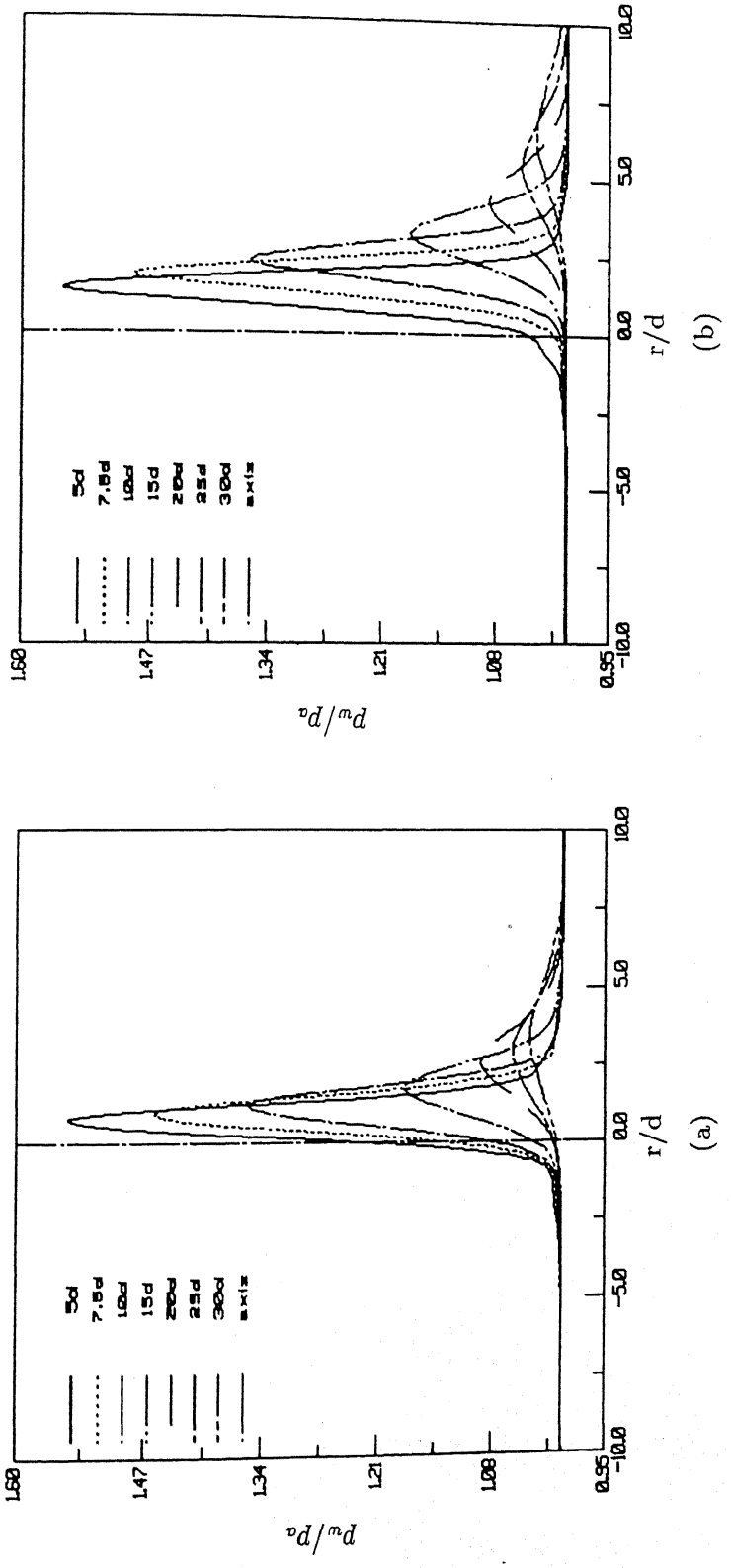

Figure 27. Wall surface pressure distribution for oblique impingement at various Dw.
a) for Me=0.8 and α=85°. b) for Me=0.8 and α=80°.

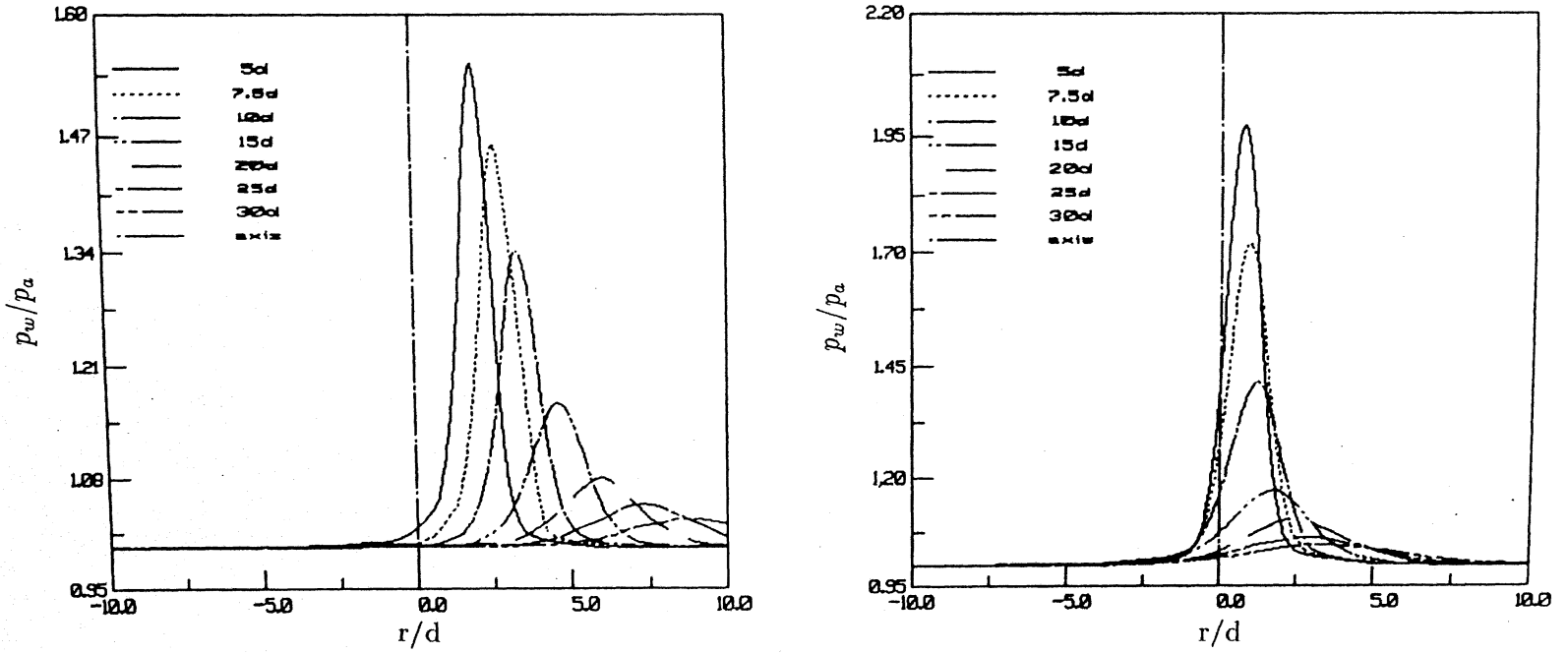

Figure 27. Wall surface pressure distribution for oblique impingement at various Dw. c) for Me=0.8 and α=75^o. d) for underexpanded flow and α=85^o.

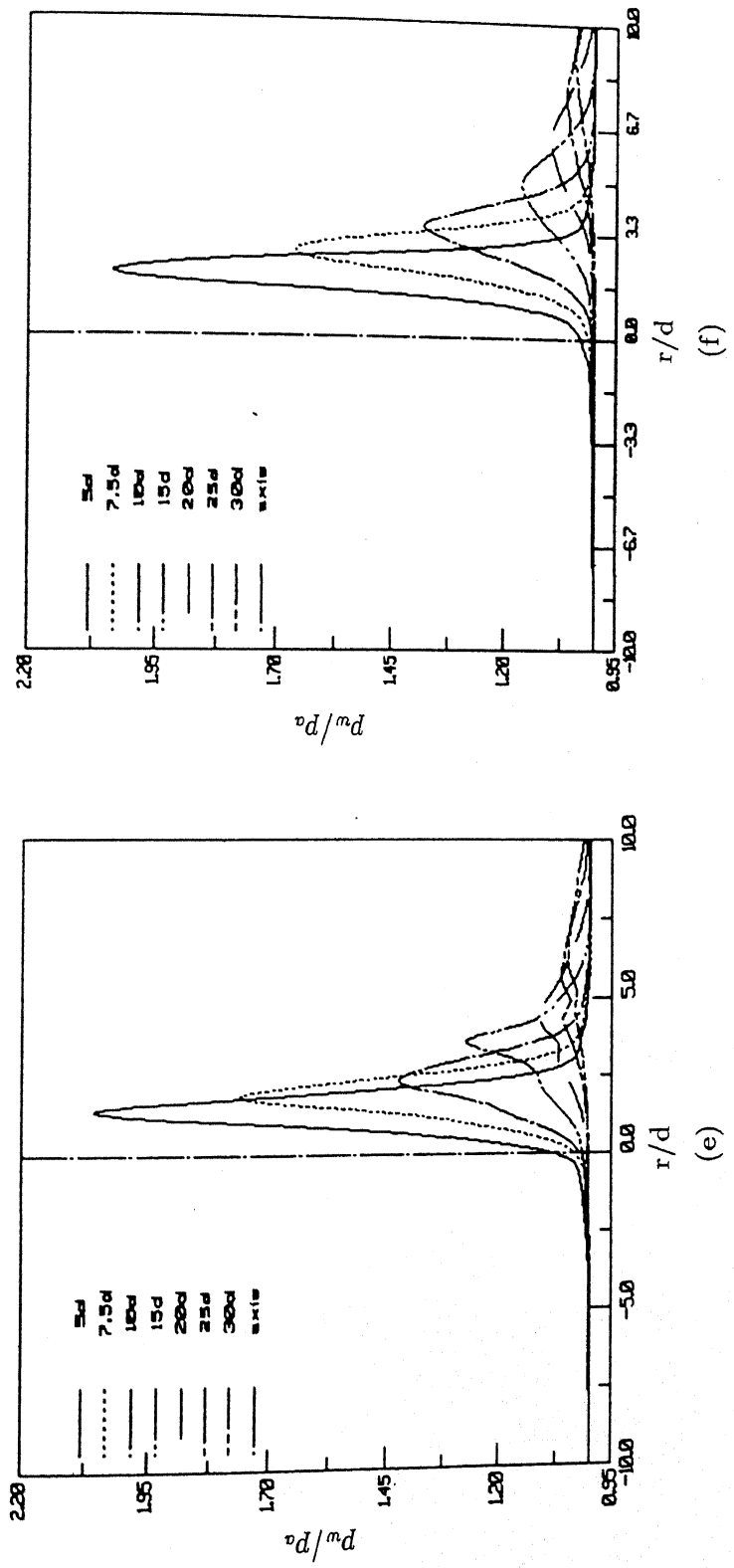

Figure 27. Wall surface pressure distribution for oblique impingement at various Dw.
e) for underexpanded flow and α=80°. f) for underexpanded flow and α=75°.

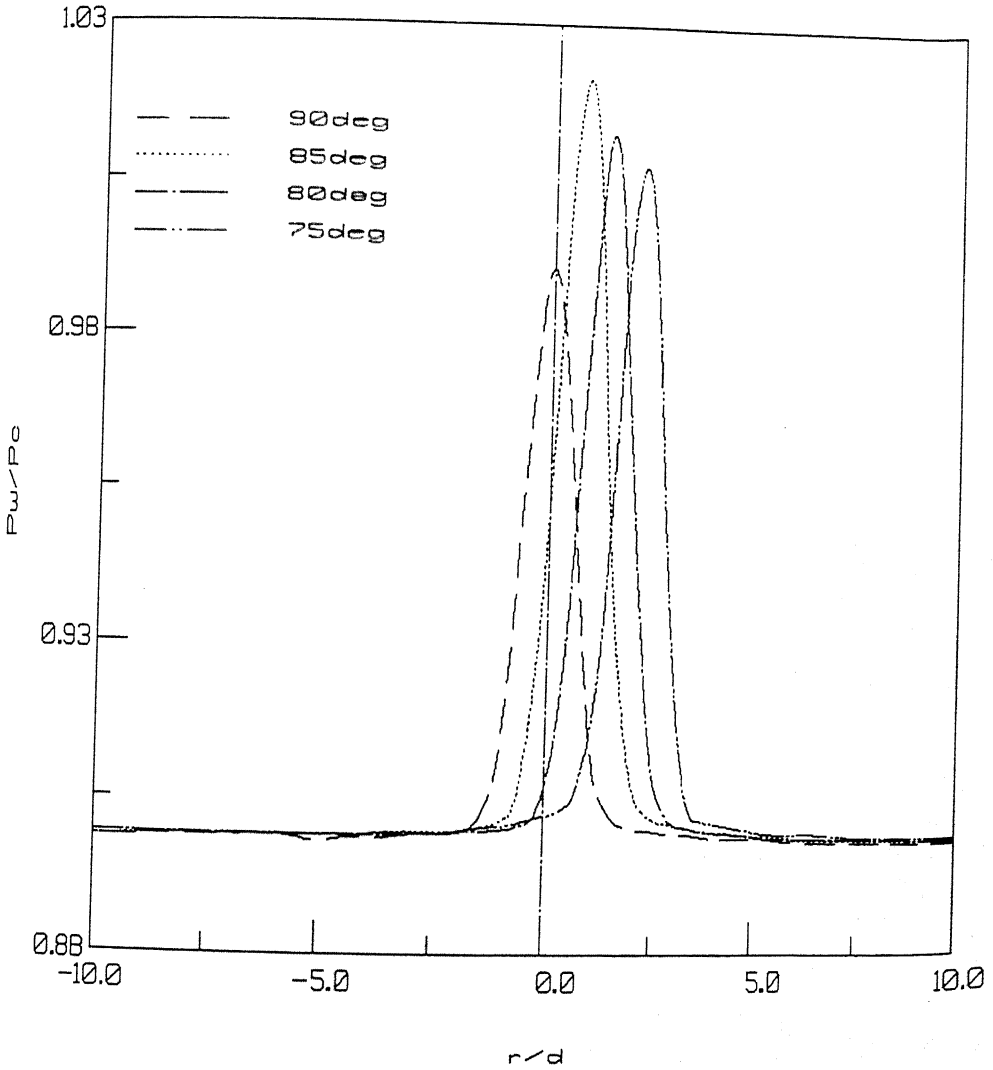

Figure 28. Wall surface pressures for oblique impingement at Dw=5d and Me=0.4.

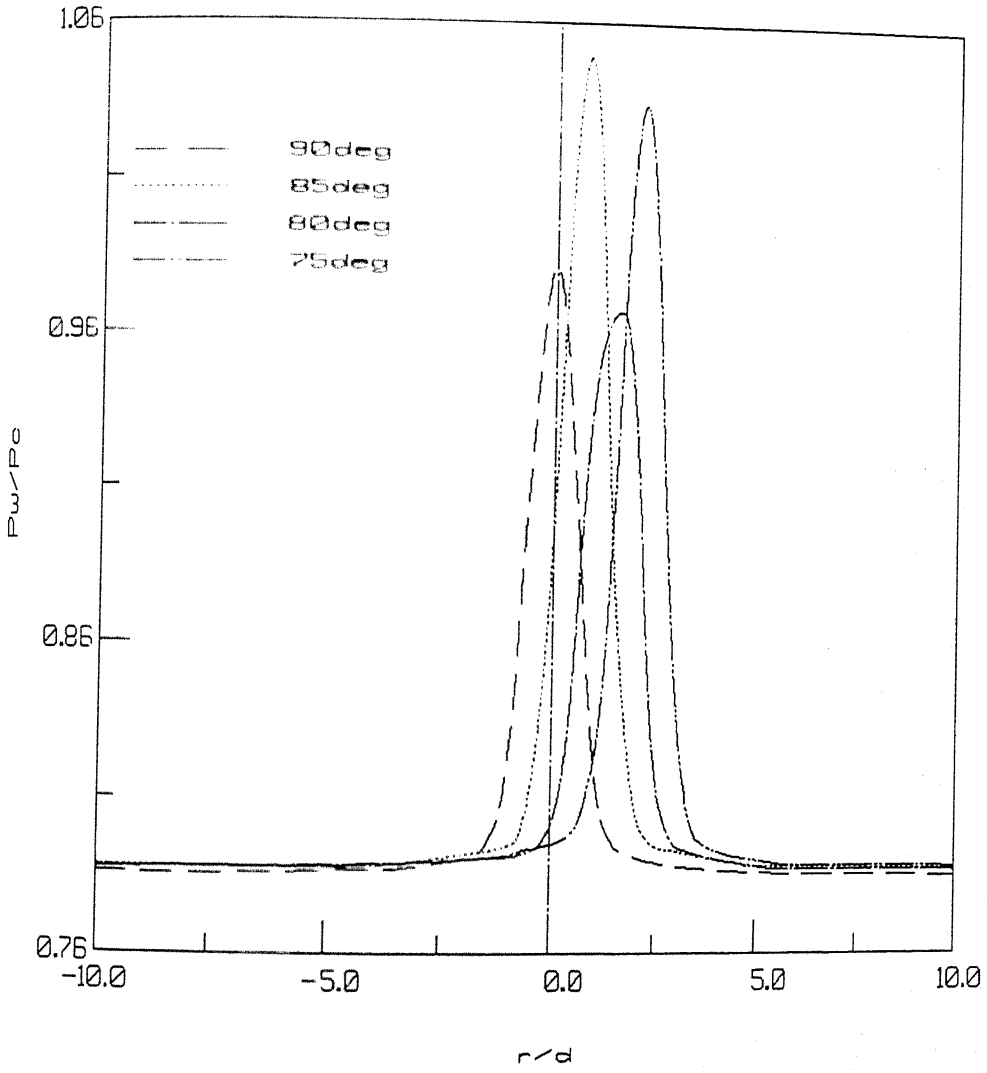

Figure 29. Wall surface pressures for oblique impingement at Dw=5d and Me=0.6.

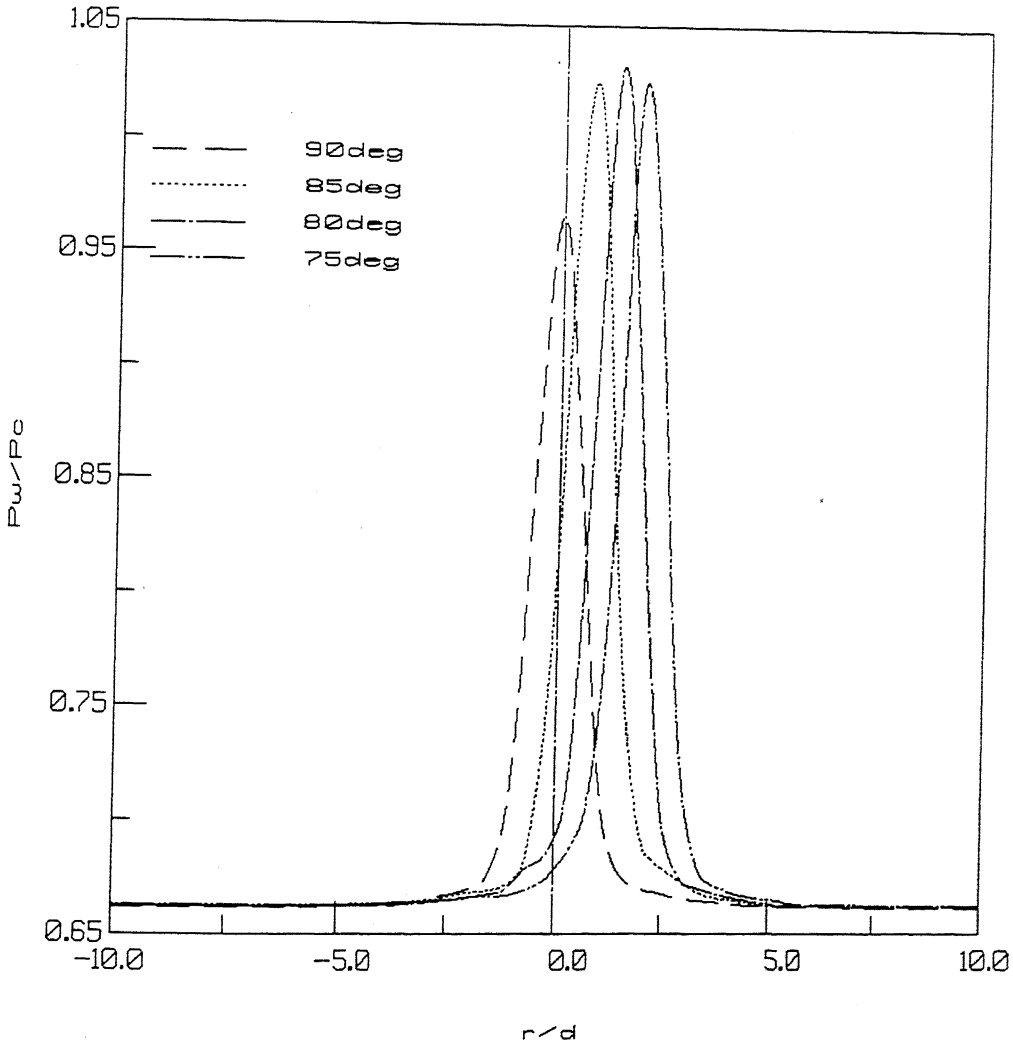

Figure 30. Wall surface pressures for oblique impingement at Dw=5d and Me=0.8.

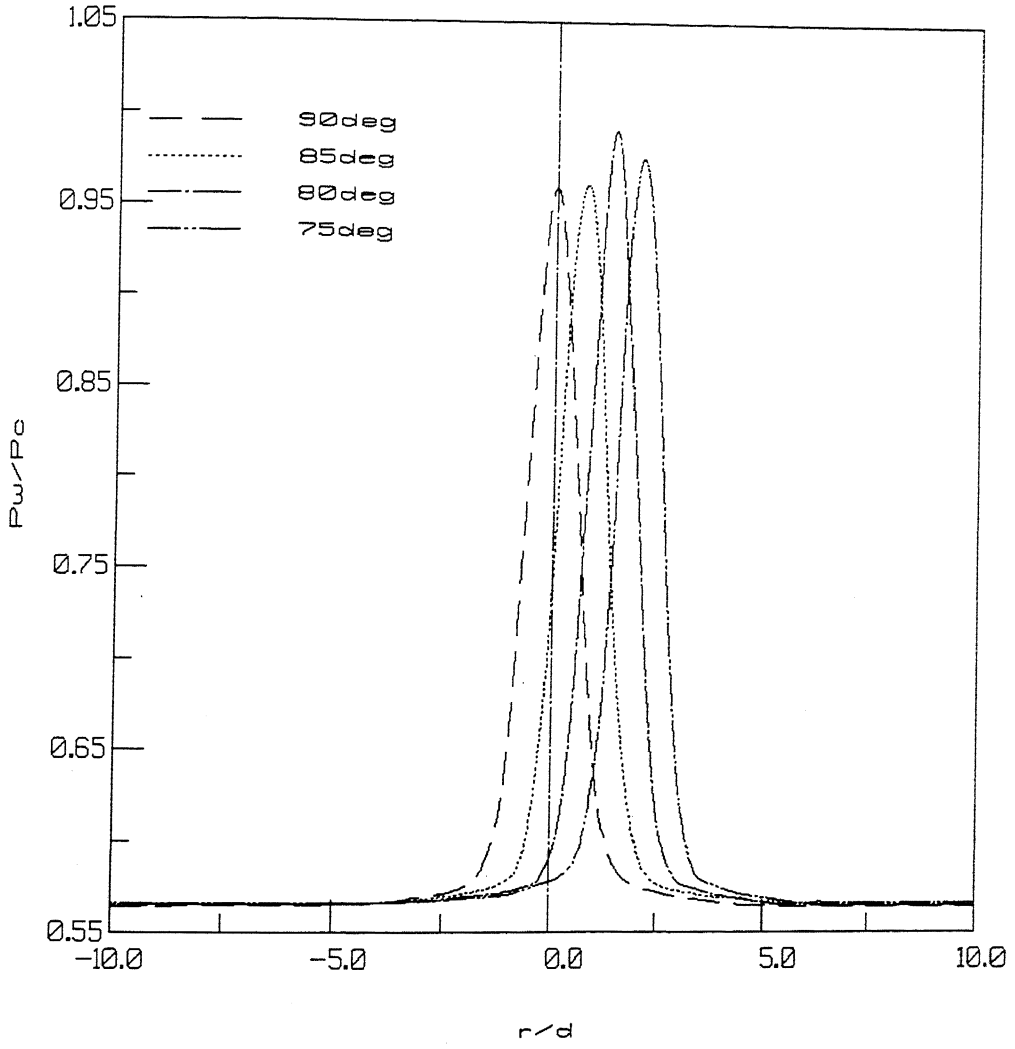

Figure 31. Wall surface pressures for oblique impingement at Dw=5d and Me=1.0.

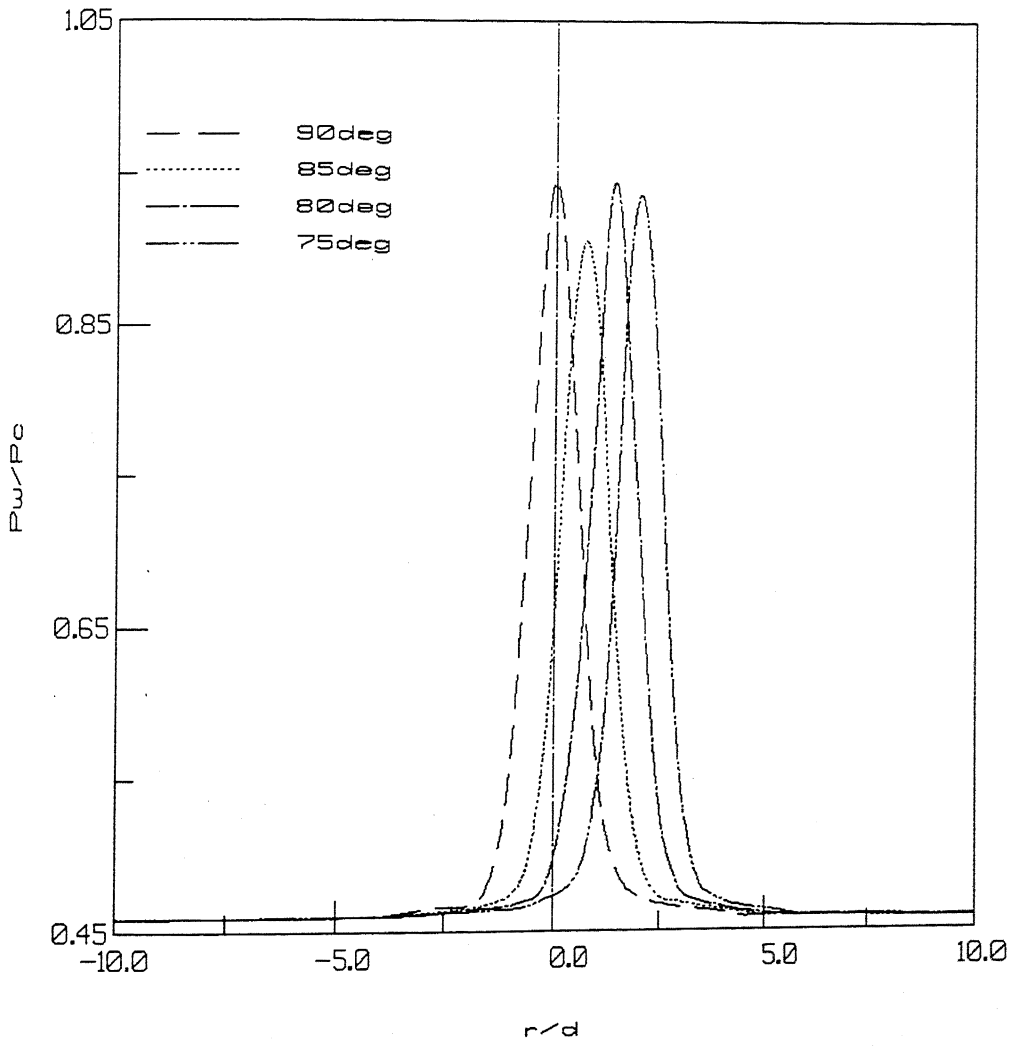

Figure 32. Wall surface pressures for oblique impingement at Dw=5d and underexpanded flow.

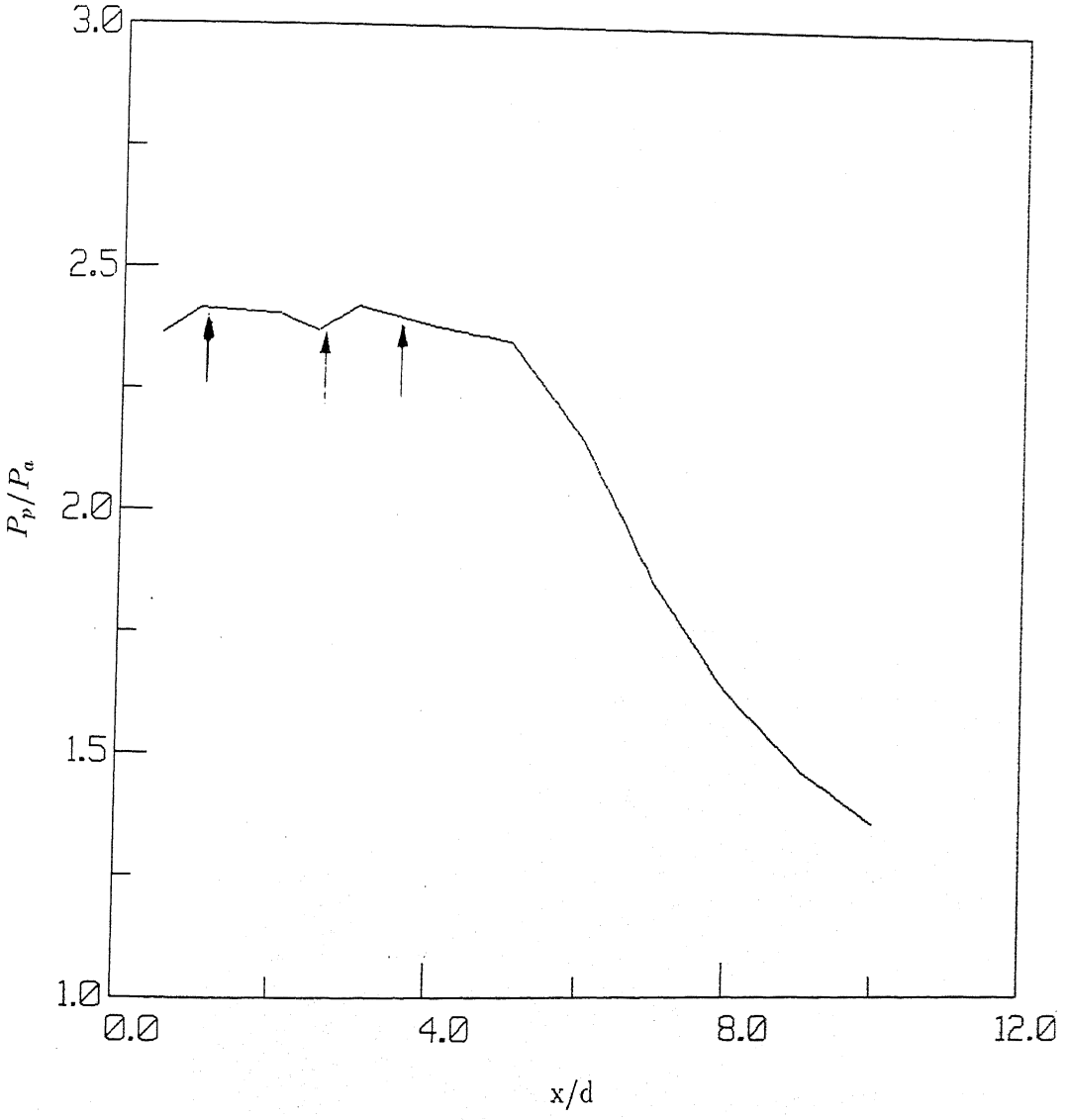

Figure 33. Axial distribution of pitot pressure of free jet for underexpanded flow, ↑ – location of free jet Mach disks from Schlieren photograph.

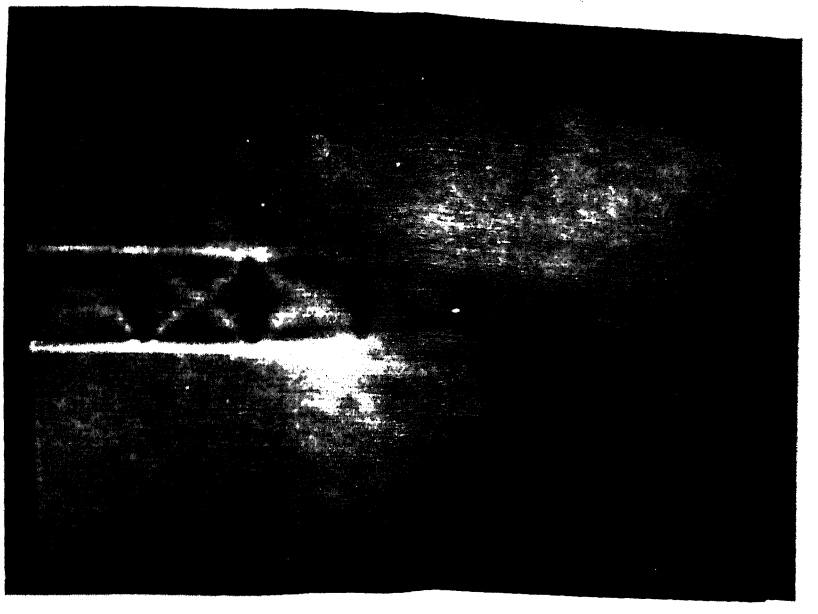

Figure 34. Schlieren picture for free jet.

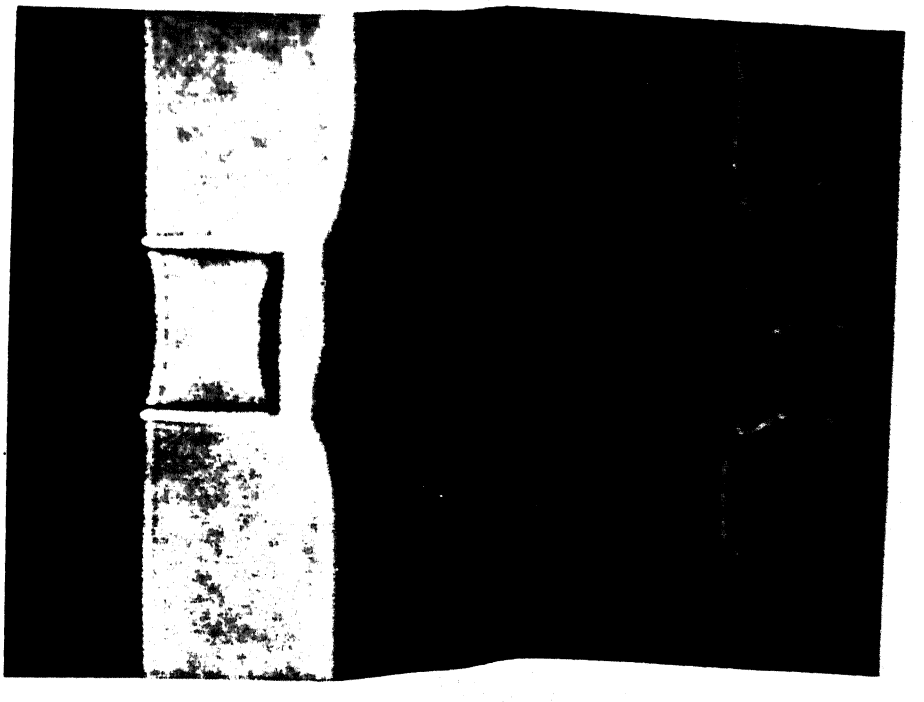

Figure 35a. Schlieren picture of normally impinging jet for D_w=1d.

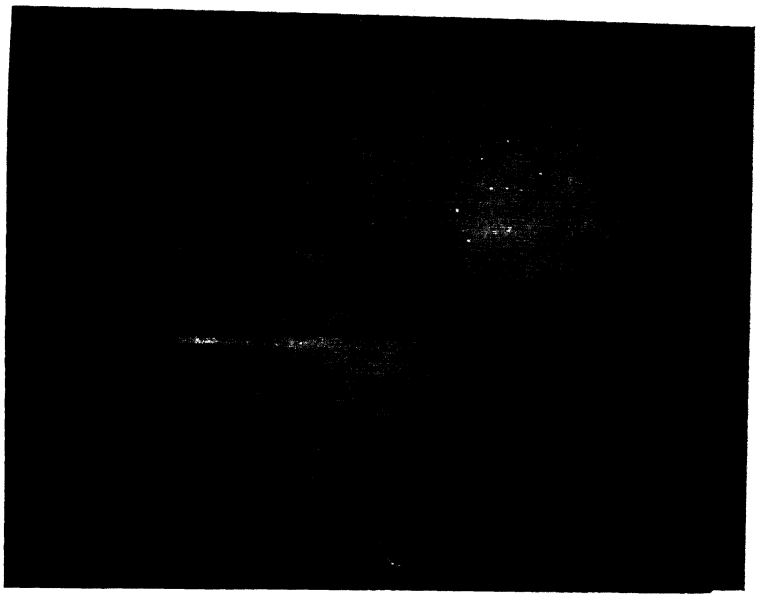

Figure 35d. Schlieren picture of normally impinging jet for D_w=5d.

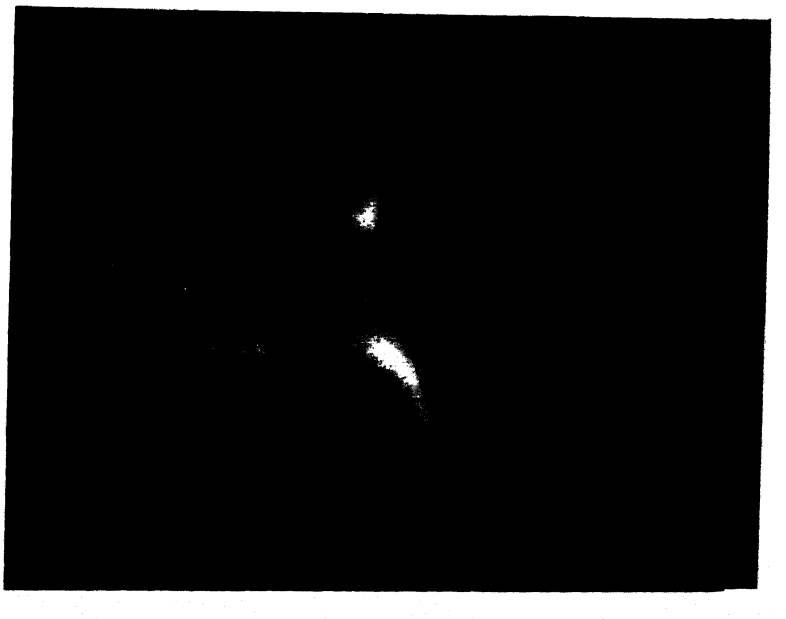

Figure 36a. Schlieren picture of obliquely impinging jet for α=85° and D_w=2d.

Figure 36b. Schlieren picture of obliquely impinging jet for α=85^o and D_w=2.5d.

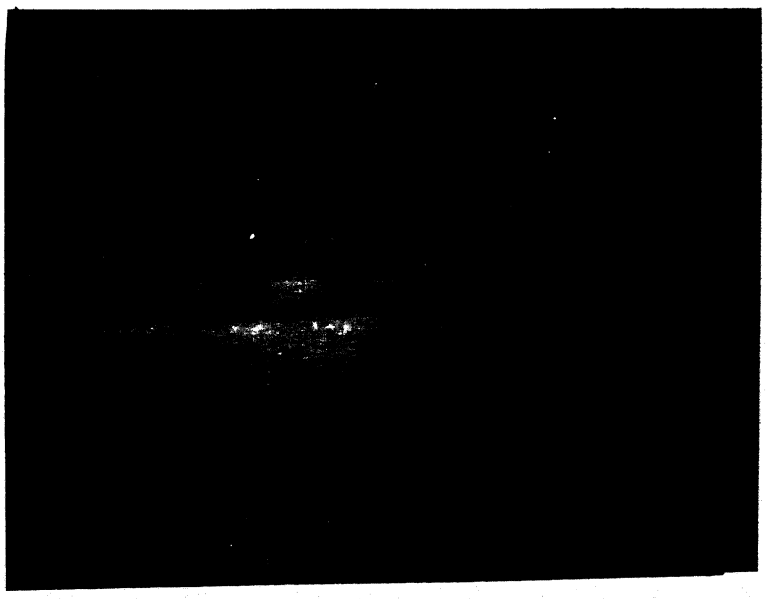

Figure 37a. Schlieren picture of obliquely impinging jet for α=85^o and D_w=5d.

Figure 37b. Schlieren picture of obliquely impinging jet for $\alpha=80^o$ and $D_w=5d$.

Figure 37c. Schlieren picture of obliquely impinging jet for $\alpha=75^o$ and $D_w=5d$.